ELECTRIC FIELD INDUCED PREDISSOCIATION OF MOLECULAR IODINE

By

Xiang Zhou

B. A. Sc. (Electrical Engineering) Tsinghua University, China

A THESIS SUBMITTED IN PARTIAL FULFILLMENT OF

THE REQUIREMENTS FOR THE DEGREE OF

MASTER OF SCIENCE

in

THE FACULTY OF GRADUATE STUDIES

PHYSICS

We accept this thesis as conforming

to the required standard

THE UNIVERSITY OF BRITISH COLUMBIA

Sept. 1991

In presenting this thesis in partial fulfilment of the requirements for an advanced degree at the University of British Columbia, I agree that the Library shall make it freely available for reference and study. I further agree that permission for extensive copying of this thesis for scholarly purposes may be granted by the head of my department or by his or her representatives. It is understood that copying or publication of this thesis for financial gain shall not be allowed without my written permission.

Department of Physics
The University of British Columbia
Vancouver, Canada

Date: Oct. 8, 1991

Abstract

Electric field induced predissociation of the B $^3\Pi_{0_u^+}$ electronic state of molecular iodine has been investigated. The flourescence spectra of I_2 , corresponding to the upper vibrational quantum mumber $v'= 4$ to $v'= 10$ have been recorded with and without a high electric field applied. Because these levels have a large natural predissociation, a specially designed high voltage cell has been built and electric fields up to 140kV/cm have been applied in order to observe the induced predissociation. By combining our results with the previous work by Dalby *et al.*[10] (from $v'= 10$ to $v'= 22$), we have the most complete predissociation data for I_2 . Both numerical and semiclassical treatments have been used to analyse the data. The form of the interacting repulsive potential curve, $^3\Pi_{1_g}$, has been revised.

Table of Contents

List of Tables

List of Figures

Acknowledgement

It gives me great pleasure to express my heartfelt thanks to my supervisor, Dr. F. W. Dalby, for his support, guidance and encouragement during the course of the project. I am very grateful to Dr. I. Ozier for his valuable instructions and suggestions. My sincere thanks are also due to Jim Booth and Alak Chanda. Their constant help and valuable suggestions were very important for the success of the project. P. Haas and J. Spencer gave many suggestions on improving the design of the high voltage cell; E. Williams did the glassblowing job. I would like to express my thanks to all of them. Thanks also goes to Dr. W. Ho for the useful conversations.

Chapter 1

Introduction

1.1 What is electric field induced predissociation

Iodine (I_2), a diatomic molecule with many desirable properties for spectroscopy study, such as convenient vapor pressure at room temperature, strong absorption spectrum and bright fluorescence spectrum in the visible region, has been intensively researched for about a century[1]. The research on the predissociation has been played an important role on the understanding of the electronic states of I_2 .

The visible fluorescence spectrum of iodine is due to a transition in the electronic structure of the molecule from the excited state $B^3\Pi_{0_u^+}$ to the ground state $X^1\Sigma_g^+$. Fig. 1.1 shows a sketch of the potential energy curves of the molecule versus the internuclear distance r, for the X and B states. Each state has a set of quantum numbers, v', J' for the B state and v'', J'' for the X state, to label the vibrational and the rotational levels respectively. Also shown in the graph is the estimated energy of the dissociative $^3\Pi_{1_g}$ state by Mulliken[21]; here we call it C state for convenience.

If the molecule is excited optically to the upper electronic level, say (B, v', J') state, it may return to the (X, v'', J'') state by radiative decay, giving rise to a fluorescence spectrum. In addition, in the presence of a dissociating potential curve like C in Fig. 1.1, the excited molecule can be transferred from the (B, v', J') state to C state by some internal or externally induced mechanism. As the result, the molecule does not emit any light, but breaks apart into two atoms[2]. The latter process is called predissociation.

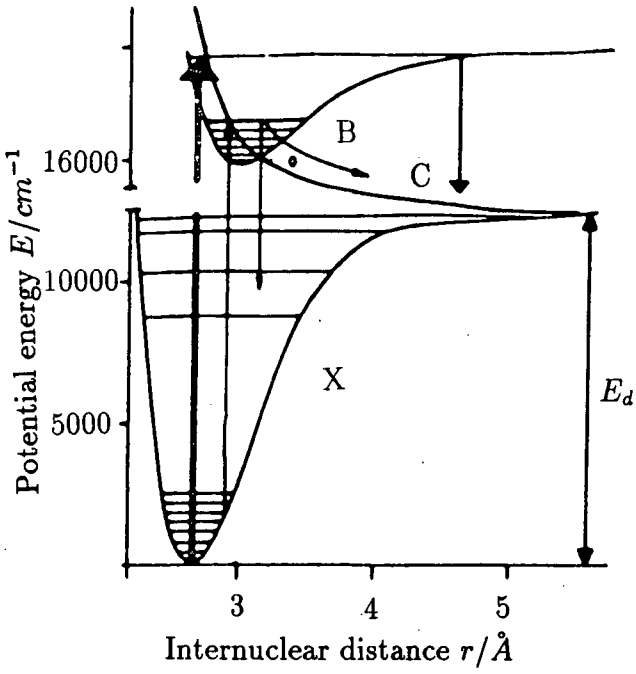

Figure 1.1: Potential curves of the X ,B and repulsive C states of molecular iodine.

When predissociation occurs, the fluorescence lines from the corresponding energy levels are broadened due to the decrease in the lifetime of the excited state, and the emission from these levels is weakened.

The predissociation may be induced by the vibration of the molecule, the coupling of the spin of the electrons with their orbital angular momentum, the rotation of the molecule, etc. This kind of predissociation is known as natural predissociation. A magnetic field or a electric field can also induce predissociation. In this work, we will mainly discuss electric field induced predissociation.

Using the experimentally measured predissociation rate constants, one can deduce information about the upper energy level B, and about the dissociative potential curve C. The latter is the main concern of this thesis.

In chapter 2, we will first discuss the usual predissociation theory. Chapter3 is about a semiclassical approach developed by Landau[3] and Child[4,5,6,7,8,9] as to obtain the

C potential curve from the predissociation data. But some of their approximations might not be appropriate for this work. We will describe our experiment apparatus in Chapter 4. Chapter 5 is devoted to experiment data and data analysis. We will discuss our numerical method and the derived C potential curve in Chapter 6.

The previous work of Dalby *et al.*[10] implies that the C potential curve is almost vertical. Assuming the C state potential curve is a straight line, the wave function of the C state for a given energy should be an as Airy function according to the solution of the Schrödinger equation for the C state(see appendix 3). The wavefunctions for the lower vibrational levels of the B potential curve can also be obtained by semiclassical expressions. With the data of the above two wavefunctions, the predissociation rate was calculated numerically.

1.2 The Franck-Condon principle in predissociation

The well-known Franck-Condon principle[2] is: *The electron jump in a molecule takes place so rapidly in comparison to the vibrational motion that immediately afterwards the nuclei still have very nearly the same relative position and velocity as before the "jump".*

The Fig. 1.2 explains the action of the Franck-Condon Principle in predissociation. When the molecule in the state B is in the neighborhood of the point of intersection I with internuclear separation r = R, a transition to the C state is possible without an appreciable alteration of position and momentum, and thus a decomposition of the molecule may take place with a significant probability. The molecule will in general carry out a number of vibrations in the stable state B before it jumps over to the unstable state C while traversing the point of intersection of the two potential curves.

If the coupling Hamiltonian is W, the predissociation rate, Γ_p, is given by the Fermi

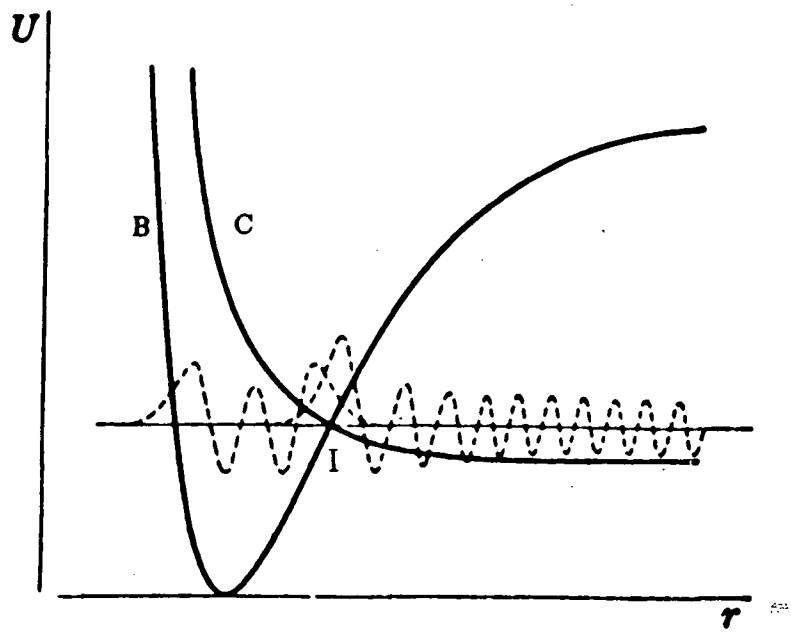

Figure 1.2: Potential curves explaining the action of the Franck-Condon principle in predissociation. The broken-line curves represent the eigenfunctions.

Golden rule:

$$\Gamma_p = \frac{2\pi}{\hbar}\left|\int \psi_m^* W \psi_n d\tau\right|^2 \tag{1.1}$$

where ψ_m is the wavefunction of the level m of the stable state B and the ψ_n is the wavefunction of the level n of the continuum C having the same energy as the level m. So, if ψ_m and ψ_n are known, the predissociation rate can be calculated.

1.3 Literature review

The natural predissociation of I_2 has been very well studied[16,17,18]. In order to calculate the natural predissociation rate Γ_N using Eq. 1.1, the vibrational Hamiltonian H_V, the rotational Hamiltonian H_R and the hyperfine Hamiltonian H_{HFS} have to be considered. Beside the H_{HFS}, all the other terms which gives non-diagonal contribution form a group called gyroscopic Hamiltonian H_G. By substituting the H_{HFS} and the H_G

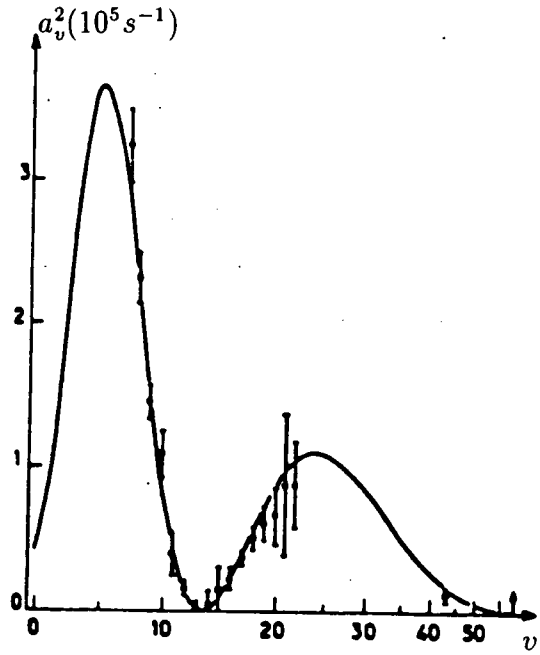

Figure 1.3: Natural predissociation constant a_v^2 given by Vigué *et al.*.

into Eq. 1.1, a complicated expression for the natural predissociation rate Γ_N has been derived[16]. Vigué gave an approximation as[22]:

$$\Gamma_N = C_v^2 J(J+1) + 4.7a_v^2 \qquad \text{for even J} \tag{1.2}$$

$$\Gamma_N = C_v^2 J(J+1) + 6.8a_v^2 \qquad \text{for odd J} \tag{1.3}$$

where C_v comes from the term H_G, and a_v from H_{HFS}. The constants 4.7 and 6.8 are obtained numerically. Fig. 1.3 and Fig. 1.4 give the natural predissociation constants a_v^2 and C_v^2 as function of vibrational quantum number v according to Vigué *et al.*[18].

As early as in 1933, Zener[20] predicted the effect of electric field induced predissociation. The Hamiltonian which causes this effect is called Stark Hamiltonian. This effect was first observed in molecular I_2 by Sullivan and Dow[19] in 1979. Fig. 1.5 shows their results.

In 1983, Dalby *et al.*[10] measured the electric field induced predissociation rate constant β as a function of vibrational quantum number v' from v'= 10 to v'= 22 in electric

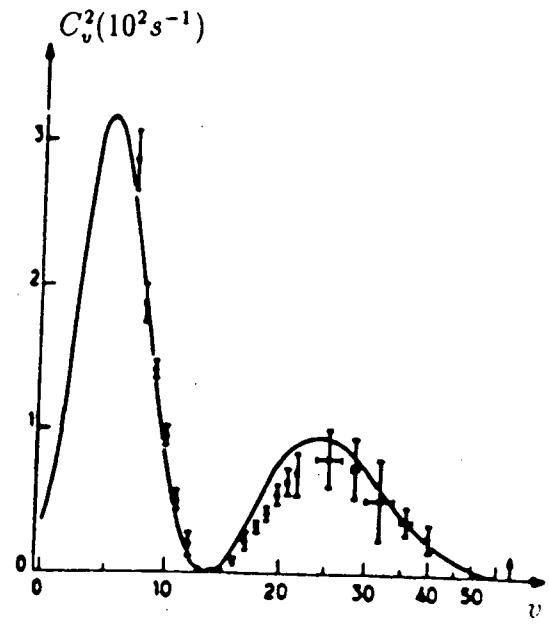

Figure 1.4: Natural predissociation constant C_v^2 given by Vigué *et al.*.

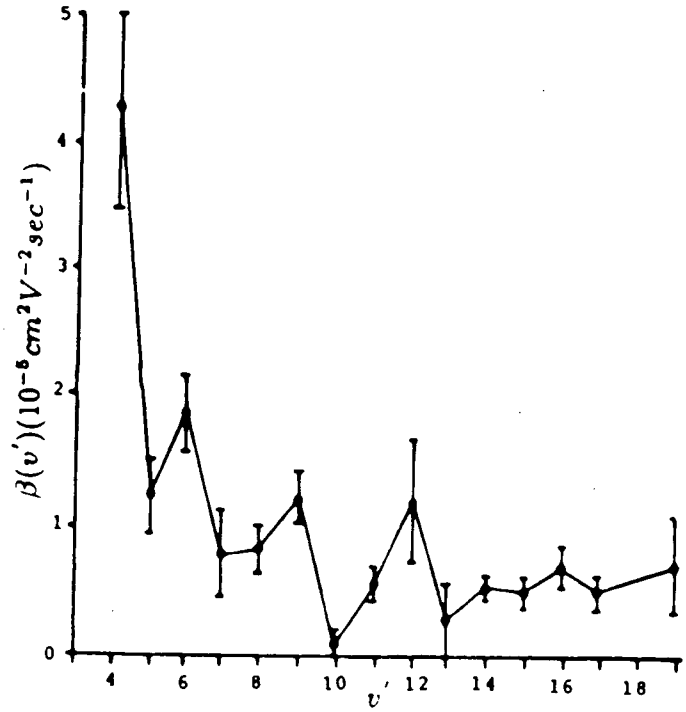

Figure 1.5: Electric field-induced predissociation rate constants given by Sullivan and Dow *et al.*.

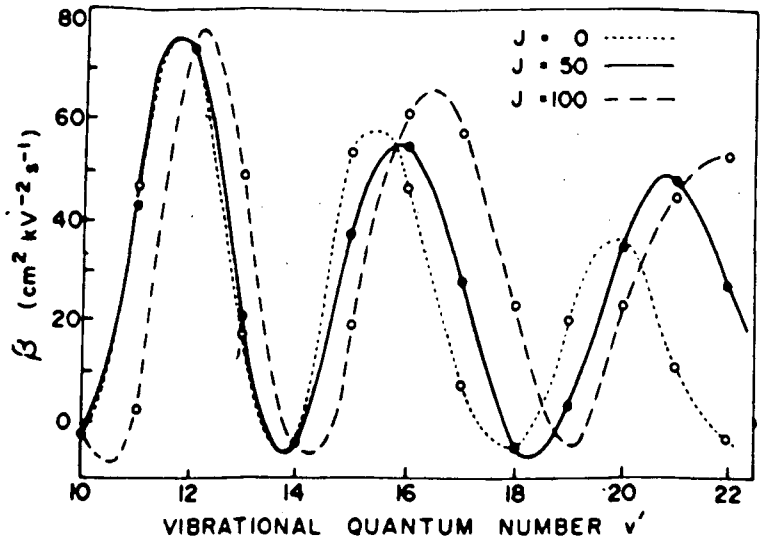

Figure 1.6: Electric field-induced predissociation rate constants given by Dalby *et al.*.

fields as high as $95kV/cm$. The electric field induced predissociation rate constant is defined as:

$$\Gamma_E = \beta E^2 \tag{1.4}$$

Where E is electric field strength and Γ_E is electric field induced predissociation rate. Dr. Dalby etc. had determined that the predissociation was caused by coupling to the $^3\Pi_{1_g}$ state which is called C state in this paper. Fig. 1.6 shows their experimental data. Using the semiclassical method suggested by Landau[3] and Child[4], they found that the curve of phases of data points against energy is close to a straight line(the word "phase" used here will be explained in detail in Section 3.2). They assumed this linear functional behavior was valid for the electric field induced predissociations of the low lying vibrational levels and derived the $^3\Pi_{1_g}$ state potential curve. Fig. 1.7 shows their assignment of $^3\Pi_{1_g}$ state.

Due to the strong natural predissociation of the low lying vibrational levels, a high

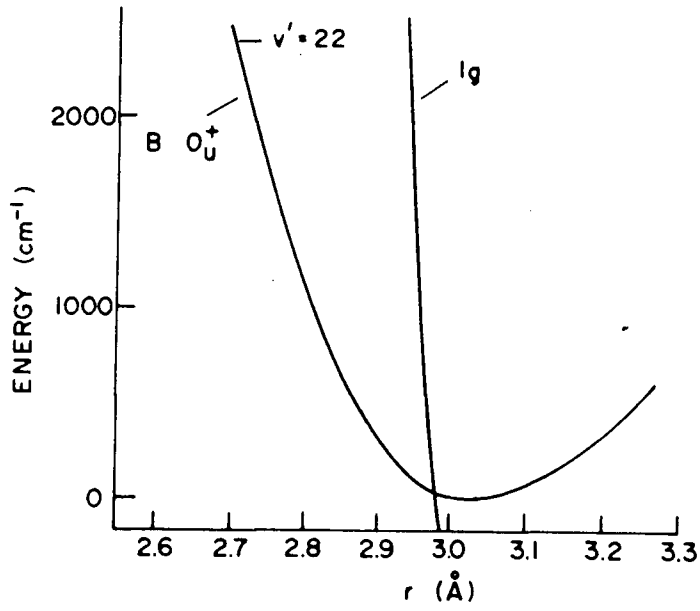

Figure 1.7: The $B\,^3\Pi_{0_u^+}$ state and the deduced $^3\Pi_{1_g}$ state potential curves given by Dalby *et al.*.

electric field is needed to measure the induced predissociation rate accurately. The task of this work is to measure the electric field induced predissociation of the B state's low lying vibrational levels and revise the $^3\Pi_{1_g}$ potential curve.

Chapter 2

Theory of Predissociation

There are a few different kinds of predissociations. Here we will only discuss Case I predissociation[2] which is defined to arise from the overlapping of a certain electronic state (that is, of its vibrational or rotational levels) by the dissociation continuum belonging to another electronic state.

In the case of diatomic molecule, we assume that the wave function of the molecule falls into the product of an electron wave function (depending on the distance between the nuclei as a parameter) and a wave function for the motion of the nuclei. According to Landau[3], Eq. 1.1 then becomes:

$$\Gamma_p \propto \frac{2\pi}{\hbar} \left| \int \chi^*_{nuc,1}(r) V(r) \chi_{nuc,2}(r) dr \right|^2 \tag{2.5}$$

where $\chi_{nuc} = r\psi_{nuc}$ (ψ_{nuc} being the wave function of the radial motion of the nuclei) and $V(r)$ is the perturbing energy.

2.1 Stark Hamiltonian and its nature

When an electric field $\vec{E}$ is applied to a molecule, a coupling happens between the electric dipole of the molecule $\vec{\mu}$ and the electric field strength $\vec{E}$. The corresponding energy operator is called the Stark Hamiltonian, which is given by

$$H_S = -\vec{\mu} \cdot \vec{E} \tag{2.6}$$

Substitute this into Eq. 2.5 and taking into account the average of the square of the direction cosine, we have:

$$\Gamma_E \propto \frac{2\pi}{\hbar} \left| \int \chi^*_{nuc,1}(r) \mu E \chi_{nuc,2}(r) \mathrm{d}r \right|^2 \tag{2.7}$$

In the case of a homonuclear diatomic molecule, the molecule has a center of symmetry. In consequence of this symmetry the electronic eigenfunctions remain either unchanged or only change sign when reflected at the center. In the first case the state to which the eigengunction belongs is called an even state(denoted by g) and in the second case an odd state(denoted by u).

2.2 The Selection rules for predissociation

Predissociation is a special case of perturbation. According to perturbation theory, the effect of a perturbation depends on the matrix element

$$V_{12} = \int \psi_1^* V \psi_2 d\tau \tag{2.8}$$

of the perturbation function V; that is it depends on the eigenfunctions ψ_1 and ψ_2 of the two states involved. The conditions for non-vanishing V_{12} are called the selection rules.

From Eq: 2.7, one can derive the selection rules for electric field induced predissociation. Here the perturbing energy is μE.

The selection rules are[16]:

1. The orbital angular momentum about the internuclear axis Λ of the two states may differ only by 0 or $\pm$ 1; that is, $\Delta\Lambda = 0, \pm 1$.

2. Both states must have the same multiplicity; that is, $\Delta S = 0$.

3. Both states must have the same component of the spin vector on the internuclear axis Σ; that is: $\Delta\Sigma = 0$.

4. The total electronic angular momentum about the internuclear axis, denoted by Ω, may differ only by 0 or $\pm$ 1; $\Delta\Omega = 0, \pm 1$.

5. The total angular momentum J of the two states may differ only by 0 or $\pm$ 1; that is, $\Delta J = 0, \pm 1$.

6. The two eigenfunctions involved must have different g - u parities; that is, electronic field only couple a g state and a u state, g$\leftrightarrow$u.

7. The two eigenfunctions involved must have different total parities; that is, +$\leftrightarrow$-.

where selection rules 1, 2 and 3 are only approximatly true.

2.3 The expression of the predissociation rate

We use n and n^* to denote the populations of the lower and upper energy levels involved in a electronic transition respectively. The equation for the upper level population is:

$$\frac{dn^*}{dt} = kIn - (\Gamma_R + \Gamma_N + \Gamma_C + \Gamma_E)n^*, \tag{2.9}$$

where k is a constant, I is laser intensity, Γ_R is the radiative decay rate, Γ_N is the natural predissociation rate, Γ_C is the collision induced predissociation rate, and Γ_E is the electric field induced predissociation rate.

When the system reaches equilibrium, we have $\frac{dn^*}{dt} = 0$, and we can get the upper level population:

$$n^* = \frac{kIn}{\Gamma_T + \Gamma_E}, \tag{2.10}$$

where

$$\Gamma_T = \Gamma_R + \Gamma_N + \Gamma_C. \tag{2.11}$$

We use E_e to denote the fluorescence intensity of the molecules in the presence of a electric field; then we have:

$$E_e = \Gamma_R n^* = \frac{kIn\Gamma_R}{\Gamma_T + \Gamma_E} \tag{2.12}$$

and obviously we have

$$E_n = \Gamma_R n^* = \frac{kIn\Gamma_R}{\Gamma_T} \tag{2.13}$$

where E_n is the fluorescence intensity with the absence of the electric field.

From the above two equations, one can easily deduce the expression for the electric field induced predissociation rate as:

$$\Gamma_E = \Gamma_T \left(\frac{E_n - E_e}{E_e} \right) \tag{2.14}$$

E_n and E_e can be measured experimentally. So if Γ_T is known, Γ_E can be calculated from the experimental data.

Chapter 3

Semi-classical Approach of Predissociation Rate

3.1 Derivation of predissociation rate

Fig. 3.8 shows effective potential energy curves of two electron states of iodine molecule. $U_J^B(r)$ is a bounded state and $U_J^C(r)$ is a dissociating potential curve. We use $\chi_B(r)$ to represent the wavefunction of the bounded state B for a given energy, and $\chi_C(r)$ the wavefunction for the dissociating C state. From equation 2.7, we have the predissociation rate:

$$\Gamma_E = \frac{2\pi}{\hbar}\left|\int \chi_B(r)\mu E\chi_C(r)dr\right|^2 \tag{3.15}$$

Because of the large masses of the nuclei their motion is quasi-classical. In general, the "transition point" I at which the transition of the system from one state to the other occurs is determined by classical conservation laws[3]. Since the total energy of the system is conserved in the transition, the condition for it to be "classically possible" is that the potential energies should be equal:

$$U_B(r) = U_C(r) \tag{3.16}$$

If the potential energy curves intersect in the classically accessible region (as shown in Fig. 3.8), transition will occur with an appreciable probability (proportional to the F-C overlap integral). Eq. 3.16 can be written in another form:

$$r_B = r_C, \quad p_B = p_C \tag{3.17}$$

where p is the momentum of the relative radial motion of the nuclei. When a transition

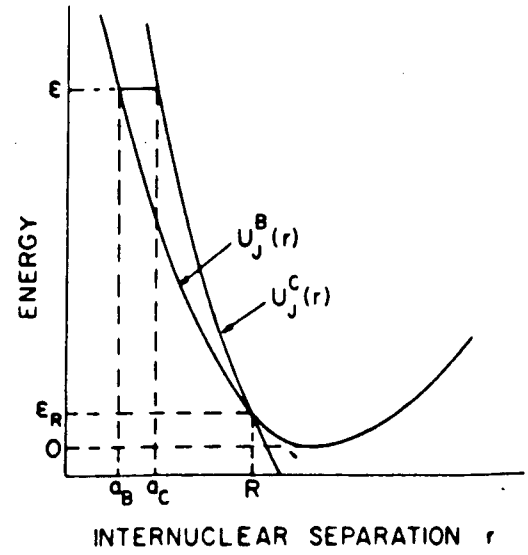

Figure 3.8: Potential curves showing symbols used in the text.

occurs, the distance between the nuclei and their relative momentum remain unchanged. The Franck-Condon principle is satisfied.

In the semiclassical approximation, we have wave functions[5]:

$$\chi_B(r) = \sqrt{\frac{2\omega}{\pi v_B}} cos\left(\frac{1}{\hbar}\int_{a_B}^{r} p_B(r')dr' - \frac{\pi}{4}\right), \tag{3.18}$$

$$\chi_C(r) = \sqrt{\frac{2}{\pi\hbar v_C}} cos\left(\frac{1}{\hbar}\int_{a_C}^{r} p_C(r')dr' - \frac{\pi}{4}\right), \tag{3.19}$$

$\chi_B(r)$ is normalized to unity. $\chi_C(r)$ is normalized by the delta function of momentum as:

$$\int \chi_p^* \chi_{p'} dr = 2\pi\hbar\,\delta(p - p') \tag{3.20}$$

v_B and the v_C are the velocities of the relative radial motion of the nuclei. By substituting these functions into Eq. 3.15 and following Landau[3], we get

$$\Gamma_E = \frac{4\omega}{\pi\hbar^2}\left|\int_0^\infty \left[cos\left(\frac{1}{\hbar}\int_{a_B}^{r} p_B(r')dr' + \frac{1}{\hbar}\int_{a_C}^{r} p_C(r')dr'\right) +\right.\right.$$

$$cos\left(\frac{1}{\hbar}\int_{a_B}^{r} p_B(r')dr' - \frac{1}{\hbar}\int_{a_C}^{r} p_C(r')dr'\right)\Big]\frac{\mu E dr}{\sqrt{v_B v_C}}\Bigg|^2 \tag{3.21}$$

In the neighborhood of the crossing point, $p_B \approx p_C$. The second term in Eq: 3.21, $\int_{a_B}^{r} p_B(r')dr' - \int_{a_C}^{r} p_C(r')dr'$, remains almost constant while the first term, $\int_{a_B}^{r} p_B(r')dr' + \int_{a_C}^{r} p_C(r')dr'$, keeps increasing. The second term makes main contribution to the integral due to the slow varying phase while the first term makes little contribution to the integral due to the fast varying phase. Only the second cosine term which has a slow varying phase is important, so that

$$\Gamma_E = \frac{4\omega}{\pi\hbar^2}\left|\int_0^{\infty} cos\left(\frac{1}{\hbar}\int_{a_B}^{r} p_B(r')dr' - \frac{1}{\hbar}\int_{a_C}^{r} p_C(r')dr'\right)\frac{\mu E dr}{\sqrt{v_B v_C}}\right|^2 \tag{3.22}$$

When r is away from the crossing point, both cosine terms have rapidly changing phases and the integral converges rapidly. So the argument of the cosine can be expanded in powers of $\xi = r - R$. Since at the point of intersection, $p_B - p_C = 0$, we have

$$\frac{1}{\hbar}\int_{a_B}^{r} p_B(r')dr' - \frac{1}{\hbar}\int_{a_C}^{r} p_C(r')dr' \approx \Phi_B - \Phi_C + \frac{1}{2}\left(\frac{dp_B}{dr'}_{|r'=R} - \frac{dp_C}{dr'}_{|r'=R}\right)\xi^2 \tag{3.23}$$

where

$$\Phi_B = \frac{1}{\hbar}\int_{a_B}^{R} p_B(r')dr' \tag{3.24}$$

$$\Phi_C = \frac{1}{\hbar}\int_{a_C}^{R} p_C(r')dr' \tag{3.25}$$

In semiclassical theory, we have

$$E = \frac{p^2}{2m} + V \tag{3.26}$$

where E is the total energy of the system, V is the potential energy, m is the reduced mass. So the above two equations can be written as

$$\Phi_B = \frac{1}{\hbar}\int_{a_B}^{R} \sqrt{2m(E - V_B(r))}dr \tag{3.27}$$

$$\Phi_C = \frac{1}{\hbar}\int_{a_C}^{R} \sqrt{2m(E - V_C(r))}dr \tag{3.28}$$

We can replace the slowly varying coefficient of the cosine by its value at $r = R$. The derivative of the momentum can be expressed in terms of the force

$$F = -\frac{dV}{dr} \tag{3.29}$$

Differentiating the equation

$$\frac{p_B^2}{2m} + V_B = \frac{p_C^2}{2m} + V_C \tag{3.30}$$

we have

$$v_B \frac{dp_B}{dr} - v_C \frac{dp_C}{dr} = F_B - F_C \tag{3.31}$$

Thus

$$\frac{1}{\hbar}\int_{a_B}^{r} p_B(r')dr' - \frac{1}{\hbar}\int_{a_C}^{r} p_C(r')dr' \approx \Phi_B - \Phi_C + \frac{F_B - F_C}{2\hbar v_R}\xi^2 \tag{3.32}$$

where v_R is the common value of the v_B and the v_C at the point of intersection. F_B and F_C are the negative derivative of the B state and C state potential curves evaluated at the crossing point $r = R$. Then the transition rate becomes

$$\Gamma_E = \frac{\omega}{\pi}\left(\frac{2\mu E}{\hbar v_R}\right)^2 \left|\int_{-\infty}^{\infty} cos(\delta + \epsilon\xi^2)d\xi\right|^2 \tag{3.33}$$

where $\delta = (\Phi_B - \Phi_C)$ and $\epsilon = (F_B - F_C)/2v_R\hbar$. This integral is well known[11]:

$$\int_0^{\infty} cos(ax^2)dx = \frac{\sqrt{\pi}}{2\sqrt{a}} cos\frac{\pi}{4} \qquad a > 0 \tag{3.34}$$

$$\int_0^{\infty} sin(ax^2)dx = \frac{\sqrt{\pi}}{2\sqrt{a}} sin\frac{\pi}{4} \qquad a > 0 \tag{3.35}$$

In the case shown in fig 3.8, one can see that $F_B - F_C < 0$ regardless of whether the intersection is to the left of the minimum or to the right. We change from $+\epsilon$ to $-\epsilon$:

$$\begin{aligned}
&\int_{-\infty}^{\infty} cos(\delta + \epsilon\xi^2)d\xi \\
&\quad = 2\int_0^{\infty} cos(-\delta - \epsilon\xi^2)d\xi \\
&\quad = 2\left[cos(-\delta)\int_0^{\infty} cos(-\epsilon\xi^2)d\xi - sin(-\delta)\int_0^{\infty} sin(-\epsilon\xi^2)d\xi\right]
\end{aligned}$$

$$
\begin{aligned}
&= 2cos\delta\frac{\sqrt{\pi}}{2\sqrt{-\epsilon}}cos\frac{\pi}{4} + sin\delta\frac{\sqrt{\pi}}{2\sqrt{-\epsilon}}sin\frac{\pi}{4} \\
&= \sqrt{\frac{\pi}{-\epsilon}}(cos\delta cos\frac{\pi}{4} + sin\delta sin\frac{\pi}{4}) \\
&= \sqrt{\frac{\pi}{-\epsilon}}cos(\delta - \frac{\pi}{4})
\end{aligned} \tag{3.36}
$$

Then Eq. 3.33 becomes:

$$\Gamma_E = \frac{4\omega\mu^2E^2}{\hbar v_R(F_C - F_B)}sin^2\left(\Phi_B - \Phi_C + \frac{\pi}{4}\right) \tag{3.37}$$

This is a little bit different with Landau's result[3] due to the different shape of the continuum potential curves concerned. If the B and C potential curves are known, the predissociation rate of different vibrational levels can be calculated accordingly. On the other hand, if we have the predissociation rates of the different vibrational levels from the experiment, and the potential of the stable state B is known, one can find the continuum C potential curve by varying its form until a set of predissociation rates agreeing with experimental data is obtained.

3.2 The method to calculate C curve directly

Using the semiclassical approximation, by means of an RKR form of integral, Child[5] has developed a way to get the continuum potential curve directly. It is as follows. If one can get the predissociation rate for the different vibrational levels, a curve of $\Gamma_E(v)$ versus the vibrational energy ε can be plotted. From Eq. 3.37 one can see that this will be a sine squared curve with slow varying amplitude. Fitting the experimental data into Eq. 3.37, one can get the phase, $\Phi = (\Phi_B - \Phi_C)$, as a function of energy. From the knowledge of this curve $\Phi(\varepsilon)$, the distance between left turning points of $V_B(r)$ and $V_C(r)$ at each vibrational level can be calculated as:

$$f(U) = (a_C - a_B) = \frac{2\hbar}{\pi(2m)^{\frac{1}{2}}}\int_{\varepsilon_R}^{U}\frac{(\partial\Phi/\partial E)dE}{[U-E]^{\frac{1}{2}}} \tag{3.38}$$

where ε_R is the energy at the crossing point as shown in Fig. 3.8. Since the values of the turning points a_B on the bound-state curve $U_B(r)$ are known[12], this completes the determination of the repulsive curve $U_C(r)$.

Chapter 4

Experiment Apparatus and Spectrum

4.1 Preparation of the experiment

4.1.1 Preparation of the high voltage cell

An original design from MIT has been modified to be suitable for our purpose. Fig. 4.9 shows the sketch of the high voltage cell. The cell has two stainless-steel parallel plates electrodes surrounded by grounded electrodes. The separation of plates can be varied. This make it possible to choose the best separation of the plates experimentally, so that we can get higher electric field without discharge. The two pyrex long arms of the cell allow us to directly compare the fluorescence from the high field region and from field free region. The ceramic rods hold the electrodes and keep them parallel to each other. The ceramic rods also separate the high voltage from the cell, so that the chance of current leakage and discharges was reduced.

4.1.2 Measurement of the separation of the plates

Referring to Eq. 3.37, one can see that for a given vibronic level, the predissociation rate Γ_E is proportional to the square of the electric field strength E, as:

$$\Gamma_E = \beta E^2 \tag{4.39}$$

where β is called predissociation rate constant. This relation had been proven by Dalby *et al.*[10]. If the potential difference between the two electrodes is V and the separation

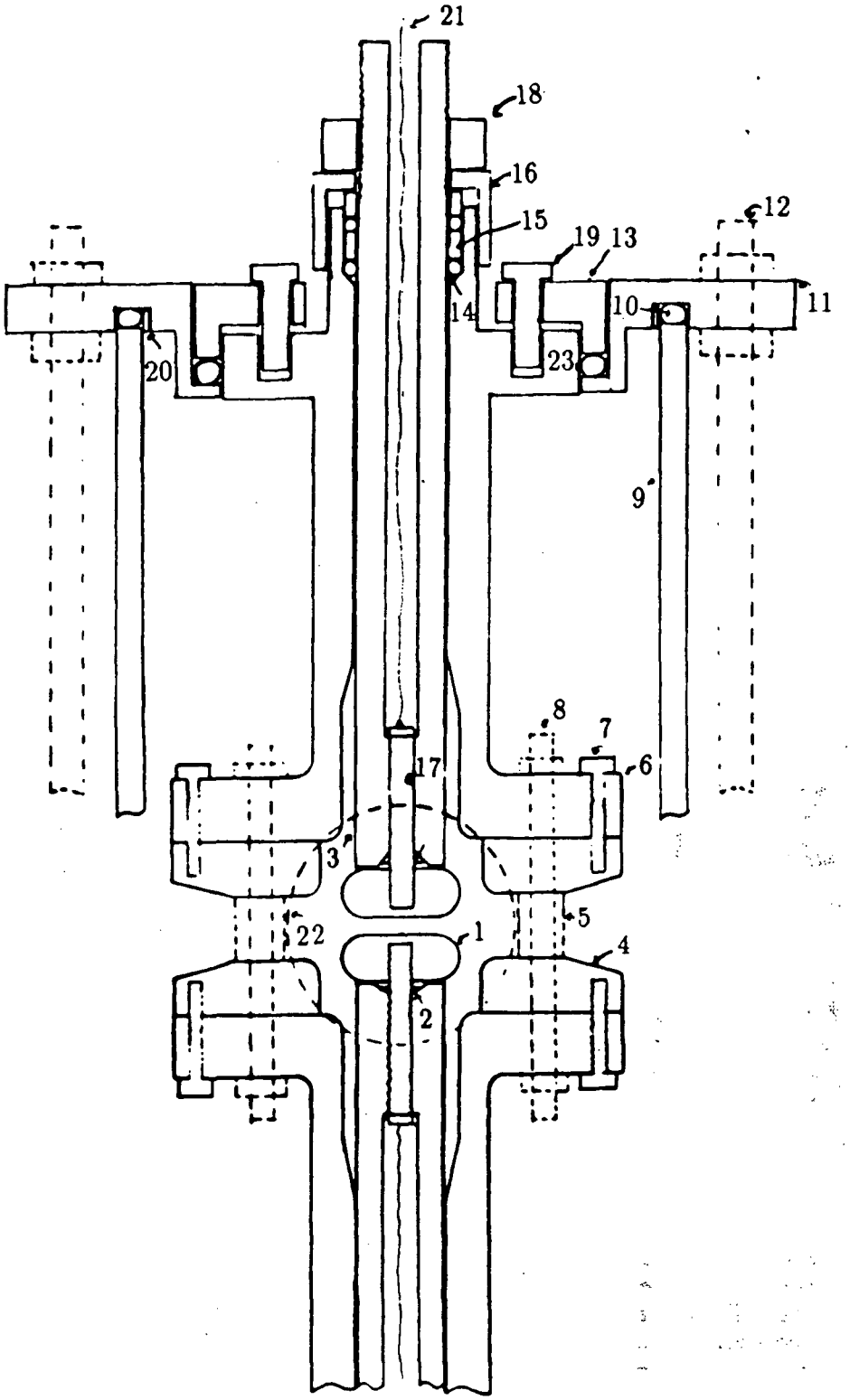

Figure 4.9: The sketch of the high voltage cell.

1: High voltage electrodes (×2, stainless steel with nickel)
2: Stycast seals (×2)
3: Insulator tubes (×2, ceramic)
4: Shields (×2, stainless steel)
5: Spacer posts (×4, stainless steel)
6: Ground electrodes (×2, stainless steel)
7: 4-40×$\frac{3}{8}$ allen head screw (×8, stainless steel)
8: 4-40 rods (×4, stainless steel)
9: Pyrex glass cylinder with two arms and two windows
10: $2\frac{1}{4} \times 2\frac{3}{8} \times \frac{1}{16}$ Viton O-rings (×2)
11: end covers (×2, stainless steel)
12: 10-32 screw rods (×4, stainless steel)
13: seal covers (×2, brass)
14: $\frac{3}{8} \times \frac{1}{2} \times \frac{1}{16}$ Viton O-ring (×4)
15: Ring spacers (×4, stainless steel)
16: fittings (×2, stainless steel)
17: 4-40×$\frac{3}{4}$ set screw (×2, stainless steel)
18: $\frac{3}{8}$-nuts (×2, brass)
19: 4-40×$\frac{5}{16}$ allen head screws (×8, stainless steel)
20: Ring protectors (×2, teflon)
21: High voltage wires (×2)
22: Pyrex glass windows (×2)

Table 4.1: Table to explain the labels used in the drawing of high voltage cell design

of the two electrodes is D, then we have:

$$E = \frac{V}{D} \tag{4.40}$$

So accurately measuring the separation of electrodes is important for getting the correct predissociation rate. Since the separation of the electrodes is small and electrodes are surrounded by shields (refer to Fig. 4.9), direct measurement is difficult.

During the assembling of the cell, a T-shape spacer has been used to keep electrodes at roughly desired separation and at the right relative position. Then a microscope accurate to 0.001mm (WHITTAM 2573, UBC 21-5410 No.9) was employed to measure the separation. The microscope was first focused on the surface of one electrode and the reading was taken. Then the microscope was moved and focused to another surface and another reading was taken. The difference of the two readings gives the separation of the electrodes.

In this way, we could measure the separation from somewhere away from the electrodes. To confirm that the measurement is correct, we put a caliper (MITUTOYO DIGIMATIC Caliper series No.500-115 460506) at approximate same distance and set the reading to 2.69±0.01 mm. Table 4.2 gives the result of the measurement of this separation. The result is 2.746±0.004mm. The errors do not cover each other, the measured value is about 2% bigger than the reading of the caliper.

This accuracy is enough for our purpose. Table 4.3 gives the result of the measurement of distance between the plates. We choose four different spots to do the measurement. The first three lines in the table give the data taken when microscope was moved from left to right, and the last three lines from right to left. The distance measured is 1.28±0.03mm. Within 2.3%, the two plates are parallel.

	1 left→right	2 right→left	3 left→right	4 right→left
left reading(mm)	2.257	4.512	1.854	4.602
right reading(mm)	5.006	1.770	4.604	1.858
difference(mm)	2.749	2.742	2.750	2.744

Table 4.2: Confirming the correction of the microscope measurement.

	first spot	second spot	at one end	the other end
left reading(mm)	4.926	4.564	3.235	3.968
right reading(mm)	6.215	5.845	4.496	5.284
difference(mm)	1.289	1.281	1.261	1.316
right reading(mm)	6.139	5.915	4.404	5.364
left reading(mm)	4.850	4.636	3.149	4.062
difference(mm)	1.289	1.279	1.255	1.302

Table 4.3: The measurement of the distance between the electrodes.

4.1.3 Calibration of the high voltage supply

From Eq. 3.37 one can see that calibration of the high voltage supply has the same importance as measurement of the separation of the electrodes. We used a Brandenburg regulated high voltage power supply Model 907, serial No. 36H, which gives up to 60 kV DC high voltage.

To calibrate it, we built a simple test circuit as in Fig. 4.10. Since the BECKMAN digital multimeter used has 10MΩ internal resistance for all the scales, if the reading of the multimeter is x volts, then the voltage supply should be:

$$\frac{R_1 + \frac{R_2 \times R_3}{R_2 + R_3}}{\frac{R_2 \times R_3}{R_2 + R_3}} \times x \text{ volts} \tag{4.41}$$

Substituting the values of three resistances, we get a conversion factor of 121. However because of the uncertainty of the values of the resistances, this result can only be used as a rough guide. The real conversion factor was measured experimentally. An F33

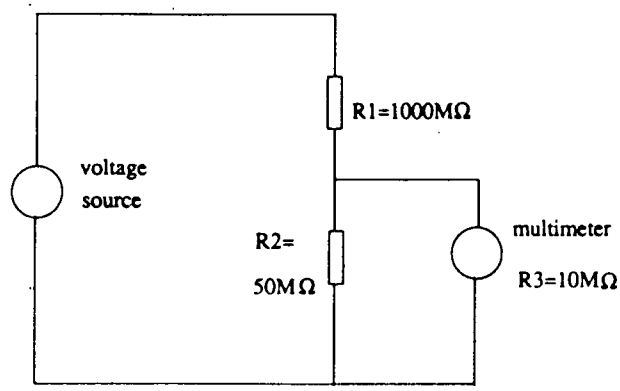

Figure 4.10: The simple test circuit.

inputvolts measured by multimeter(V)	outputvolts measured by testcircuit(V)	ratio
10.080±0.001	0.0896±0.0001	112.50
6.207±0.001	0.0550±0.0002	112.85
4.212±0.001	0.0374±0.0002	112.62

Table 4.4: Measurement of the conversion factor of the test circuit.

Function Generator (ser. No. 0557) was used as DC voltage source. The output was first measured directly by the digital multimeter, then the multimeter was connected as in Fig. 4.10, and another reading was taken. The ratio gives the conversion factor. Table 4.4 gives the data. The ratio measured was 112.6±0.2.

Then the voltage source was replaced by the high voltage supply. Table 4.5 shows the calibration result. The procedure for the calibration was: the power supply was first set to 1kV visually and the reading from test circuit was taken, then to 2kV, 3kV, $\cdots$, until 20kV. The power supply was set randomly to a few previously measured values to test the repeatability of visually setting.(This is the biggest error source.) The data are shown in the Table 4.5. When 20kV was applied to the test circuit, the current that flowed

panel reading (±0.1kV)	first meas. (±0.01)	second meas. (±0.01)	third meas. (±0.01)	calibrated (kV)
1	9.11			1.02
2	18.80	19.17	18.82	2.13±0.02
3	27.80	28.00		3.14±0.02
4	36.92			4.16
5	45.40	45.88	45.53	5.14±0.03
6	54.64			6.15
7	64.10			7.22
8	73.30	73.45	73.15	8.25±0.02
9	82.51			9.29
10	91.70	91.80	91.62	10.33±0.01
11	101.30			11.41
12	110.42	110.78	111.17	12.48±0.04
13	119.69	120.48		13.52±0.06
14	129.20	128.49		14.51±0.06
18	167.80	168.40		18.93±0.05
19	177.70	177.78		20.01±0.01
20	188.00			21.17

Table 4.5: Calibration of the power supply.

through the circuit was about 0.02mA, which produced about 0.4W heat, (negligible). Fig 4.11 fits the data to a straight line, so we get the calibration formula

$$V = 1.052V_p - 0.110 \tag{4.42}$$

where V_p is the front panel reading of the voltage supply and V is the calibrated value.

4.1.4 Design of the pumping system

Fig. 4.12 shows the sketch of the pumping and the filling system including an oil diffusion pump, a mechanical pump as fore pump, air cooling fan, a cold trap with O-ring seal, an ion gauge with controller(Varian 843), an iodine cell and an opening to connect the high voltage cell.

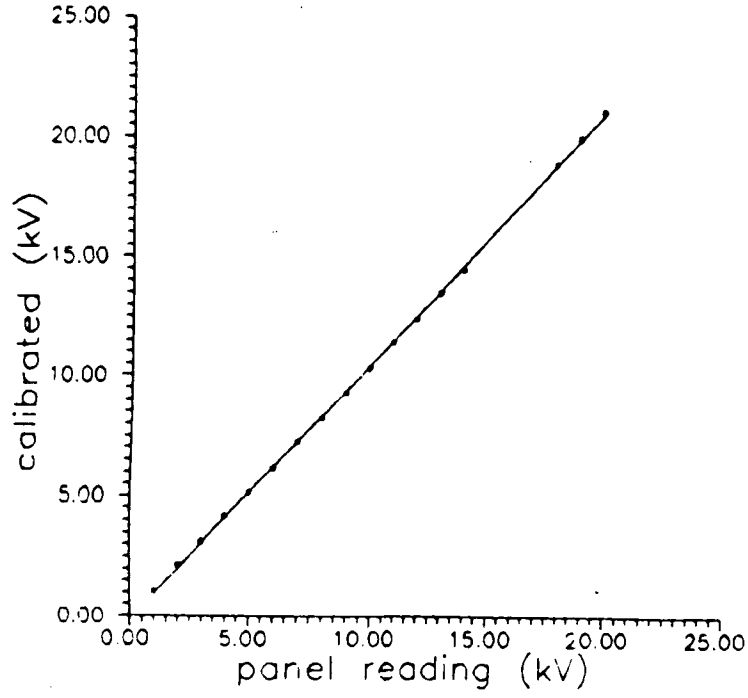

Figure 4.11: The calibration curve of the power supply.

There are a few important points to keep in mind when using the pump to get a good vacuum inside the cell.

- The temperature of the oil has to be right to get good performance of the pump. We have measured the pumping speed at different temperatures, Fig. 4.13 shows the result. For the NEOYACSY oil used, the best voltage applied to the heater is about 85 volts.

- During the experiment, the cold trap has to be kept at liquid nitrogen temperature all the times to prevent oil vapor from feeding back to sample cell. At night, valves sc1 and sc5(Fig: 4.12) were closed to keep the cell at low pressure.

- There should not be any blind holes inside the cell. Otherwise they might slowly degas for a long time.

- The cell has to be thoroughly pumped out and baked at 100°C for 2 days before

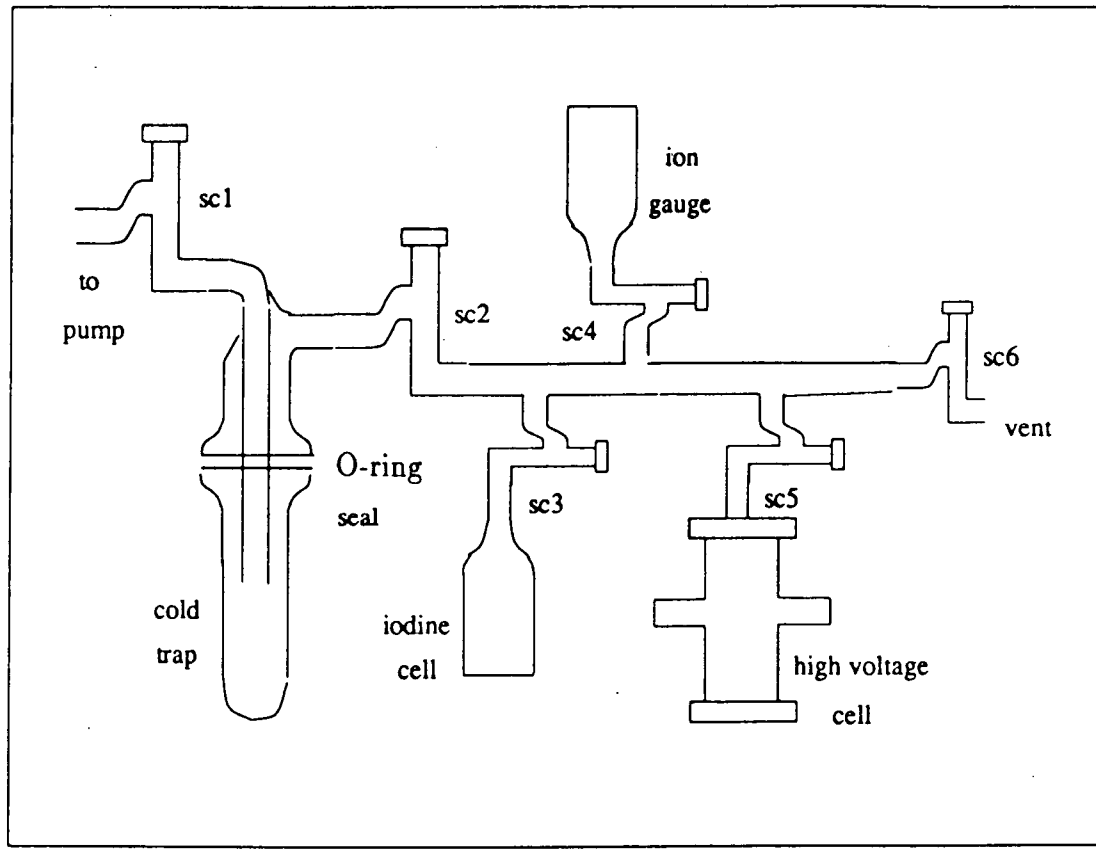

Figure 4.12: The design of the pumping and filling system.

use.

- Since I_2 might attack vacuum grease, we made the cell grease free.

4.1.5 Getting clean I_2

The I_2 cell was first baked and pumped out at 150°C for 8 hours. Then an I_2 crystal was placed inside it. Since I_2 crystal had absorbed water vapor when it was exposed to air, it is necessary to clean the I_2 . Since the vapor pressure of I_2 at 0°C is 0.03 torr while for water it is 4.6 torr[13], this difference, a factor of 150, makes it possible to separate I_2 and water. While the I_2 cell was kept at 0°C, the valve sc3(refer to Fig. 4.12) was

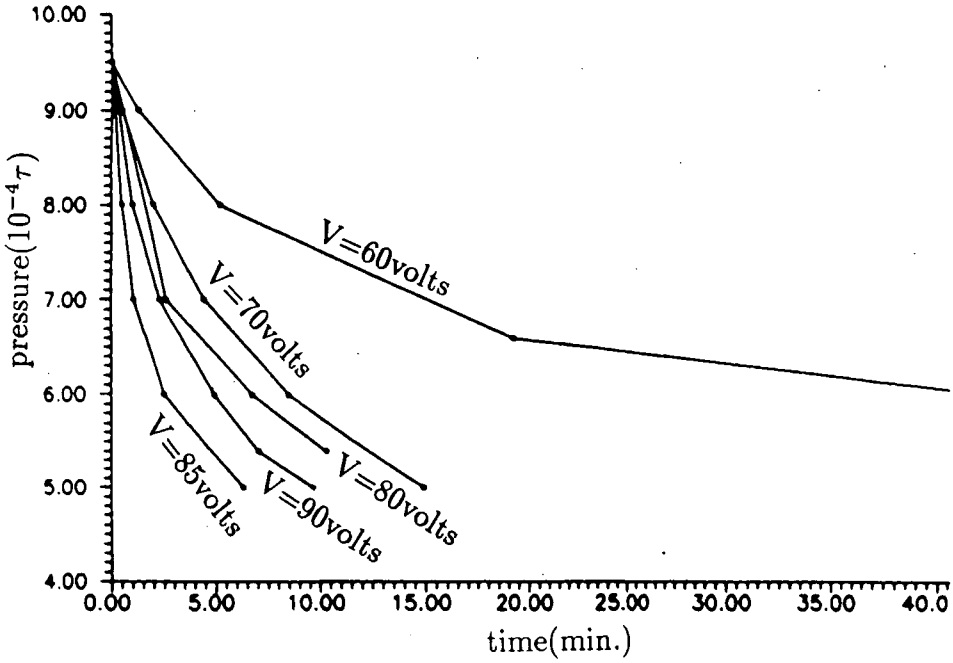

Figure 4.13: The performance of the oil diffusion pump at different temperature.

slowly opened, the water vapor and some I_2 vapor was pumped out. Then the valve sc3 was closed. Since the cold trap was at liquid nitrogen temperature, most of the I_2 vapor was trapped there so it did not harm the pump. Then the I_2 cell was heated up until all the I_2 molecules were redistributed. This was to release any water trapped inside the I_2 crystal. The cell was then pumped out again at 0°C. The same procedure was repeated 3 or 4 times, to prepare the I_2 for use in the experiment.

4.2 Experimental apparatus

A block diagram of the experimental arrangement used for measuring the electric field induced predissociation in the $B\,^3\Pi_{0_u^+}$ state of molecular iodine is shown in Fig. 4.14.

A Coherent CR-15 SG argon ion laser was tuned to the 5145 Å line, and an output power of 6.5W was used to pump a Coherent CR-699-21 scanning ring dye laser. DCM dye was used which allowed the laser to cover from 14500 cm^{-1} to 16200 cm^{-1} with

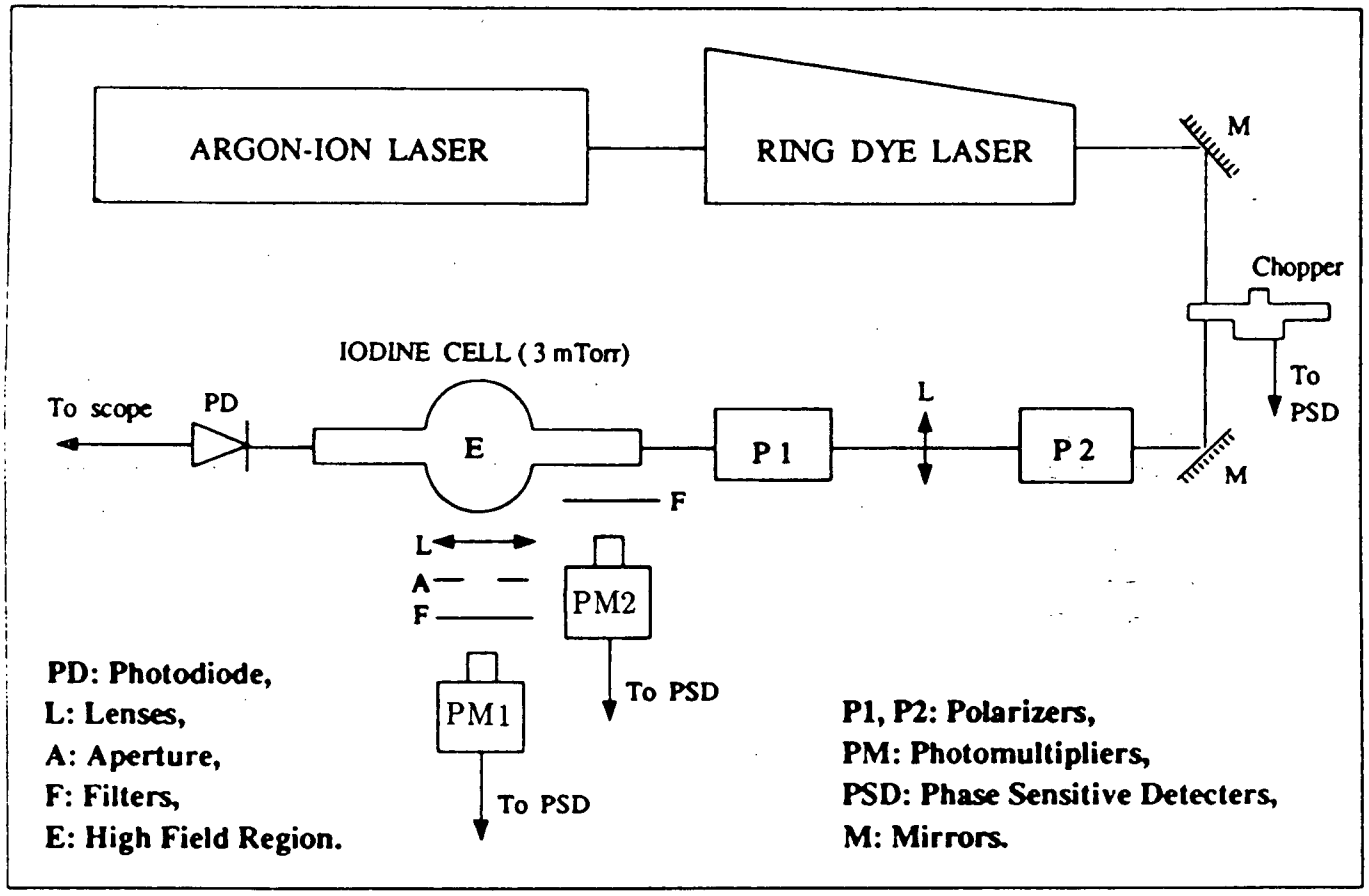

Figure 4.14: Experimental arrangement.

a peak power of 400 mW. A chopper working at 1.8 kHz chopped the laser beam and sent a reference signal to the lock-in amplifiers. With two polarizer P1 and P2 we could decrease the laser intensity to any level we needed and the laser light was polarized parallel to the applied electric field to minimize the Hanle effect[22, pages 70 - 71]. A 31 cm focal length lens focused the beam down to one-third of the electrodes separation and ensured that laser beam did not hit the electrodes. Photomultipliers PMT1 (EMI 9558 B) and PMT2 (EMI 9558 QB), both with Corning CS2-64 red pass filters and 100 kΩ loads, were used to detect the fluorescence from high field region E_e or E_n and field free region N_e or N_n respectively. Here subscript n means that the high field is off and e means that it is on. To ensure that PMT1 only saw the signal from between the plates, a lens with 3.5 cm focal length was placed 4.6 cm away from the center of the plates. A 3 times magnified image was obtained at the back focal area where a 2×2 cm aperture was employed to let only center $\frac{1}{7}$ of the total fluorescence pass. The outputs from two PMTs were sent to two PAR model 121 lock-in amplifiers and were recorded by a double line recorder(PM8252A). A third lock-in amplifier(PAR model 128) and another PM8252A double line recorder were used to record the difference signal $N_n - E_n$ or $N_e - E_e$ electronically. A photodiode was placed behind the iodine cell so that we could monitor the laser intensity on an oscilloscope.

4.3 Experimental procedure

During the experiment, the high voltage cell was connected to a pumping station shown in Fig. 4.12. The cell was first thoroughly pumped out and baked at 100°C for 2 days. The pressure measured by the ion gauge was as low as 1.2×10^{-5} torr. Then valve sc5 was closed and the I_2 in the iodine cell was given a final clean up. It was pumped out at room temperature for 5 sec.; then valve sc2 was closed and valve sc5 was open; the high

voltage cell was filled at room temperature for 30 sec. Then both valve sc3 and valve sc5 were closed and the filling was completed. Since stainless steel absorbs a lot of I_2 , we had to fill the high voltage cell at a pressure a lot higher than needed; otherwise there wouldn't be enough I_2 inside the high voltage cell.

The chopped laser beam was sent in, the laser was turned to a fluorescence line so the trace of laser beam inside the cell could be observed. The beam was visually set to between the plates and the reflected beam from the far end window was also arranged to go back between the plates. Scanning the laser frequency, without the electric field, the spectrum from field-free region labeled N_n, and that from between the plates E_n were recorded, the difference signal $D_n = N_n - E_n$ was also recorded. A conversion factor, *Con*, was also measured to reflect the gain difference between model 121 and model 128 lock-in amplifiers. Then a high voltage was applied to electrodes so that an electric field was established between the plates. We recorded another set of the spectra: N_e, E_e and D_e. We have two slightly different ways to calculate predissociation rate.

Refer to Eq. 2.14. Experimentally we cannot measure E_n and E_e at the same time. Unfortunately during two different scans, laser intensity and I_2 concentration may change slightly. To correct this we had to multiply the ratio $\frac{N_e}{N_n}$ to E_n. Eq. 2.14 becomes:

$$\beta E^2 = \Gamma_T \times \frac{E_n \times \frac{N_e}{N_n} - E_e}{E_e} \tag{4.43}$$

Denoting

$$I_n = \frac{N_e}{N_n} \tag{4.44}$$

$$I_e = \frac{E_e}{E_n} \tag{4.45}$$

we get

$$\beta = \frac{\Gamma_T}{E^2} \times \frac{I_n - I_e}{I_e} \tag{4.46}$$

E is the electric field strength which equal to voltage applied to electrodes V over separation of the plates D. We call this RATIO method.

When the predissociation rate is small. *ie.* $I_n \approx I_e$, the term $I_n - I_e$ may induce a large error, but if we can measure the $I_n - I_e$ electronically, this error might be reduced. The other method called DIFFERENCE method was an attempt to reduce this error. We adjusted the gain difference of the two photo multiplier tubes until $E_n = N_n$, the Eq. 4.43 becomes:

$$\beta = \frac{\Gamma_T}{E^2} \times \frac{N_e - E_e}{E_e} \tag{4.47}$$

Since $D_e = N_e - E_e$, we have:

$$\beta = \frac{\Gamma_T}{E^2} \times \frac{D_e}{E_e \times Con} \tag{4.48}$$

The conversion factor, Con, was obtained by taking the ratio of the outputs of the two lock-in amplifiers when their inputs were exactly same.

Chapter 5

Spectrum and Data Analysis

5.1 Sample spectrum

Fig. 5.15 is the spectrum showing an electric field induced predissociation effect. The number in the bracket is the rotational quantum number; v' is the upper level vibrational quantum number; and v'' is the lower level vibrational quantum number. When an electric field of the order of 140 kV/cm was applied to the I_2 molecules, the fluorescence dimmed. Fig. 5.16 illustrates the DIFFERENCE method. When spectrum dimmed, the difference signal, D_e, increased. There is a 3 mm offset between the horizontal scales in the upper and lower drawings.

5.2 Impurities

Although the high voltage cell had been baked before use, due to the complicated structure of the cell, there are a few reasons that there may be impurities in the cell.

- When there is a discharge, foreign gas can be knocked out of the electrodes.
- The cell contains different materials, making it impossible to bake it to a very high temperature, so that there might be still some outgasing going on in the cell.
- There might be some very small leaks which we didn't find.

The effect of impurities in the cell is that, for the different vibrational and rotational levels, the relative intensities of the fluorescence signal are changed and the over all

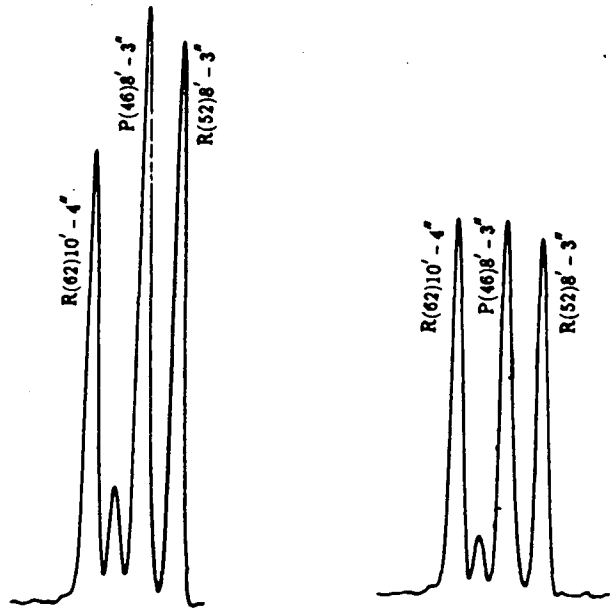

a: ZERO FIELD b: 140 kV/cm

Figure 5.15: The spectrum showing the electric field induced predissociation effect.

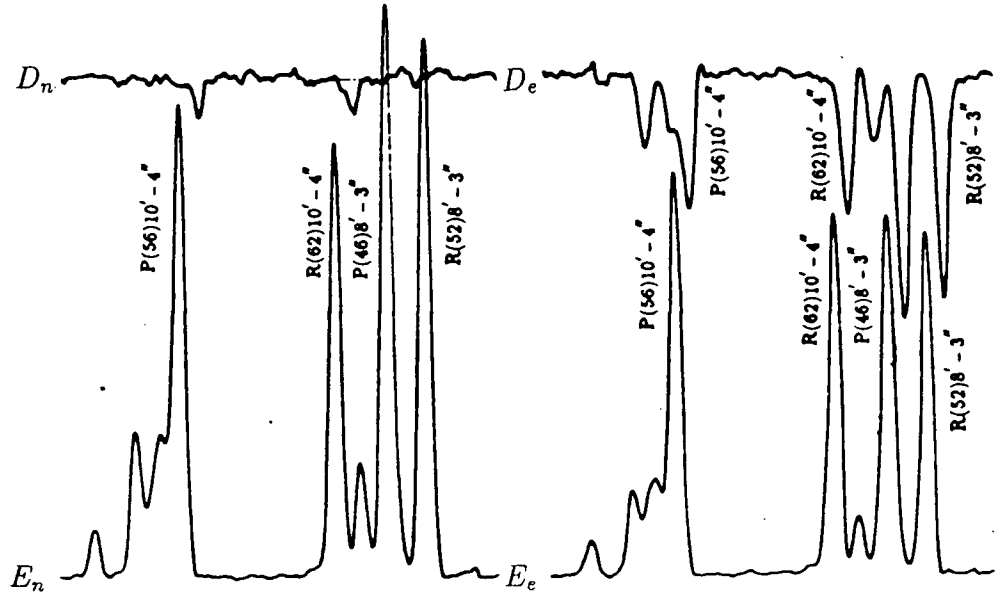

a: ZERO FIELD b: 140 kV/cm

Figure 5.16: The spectrum showing the direct measurement of the difference signal.

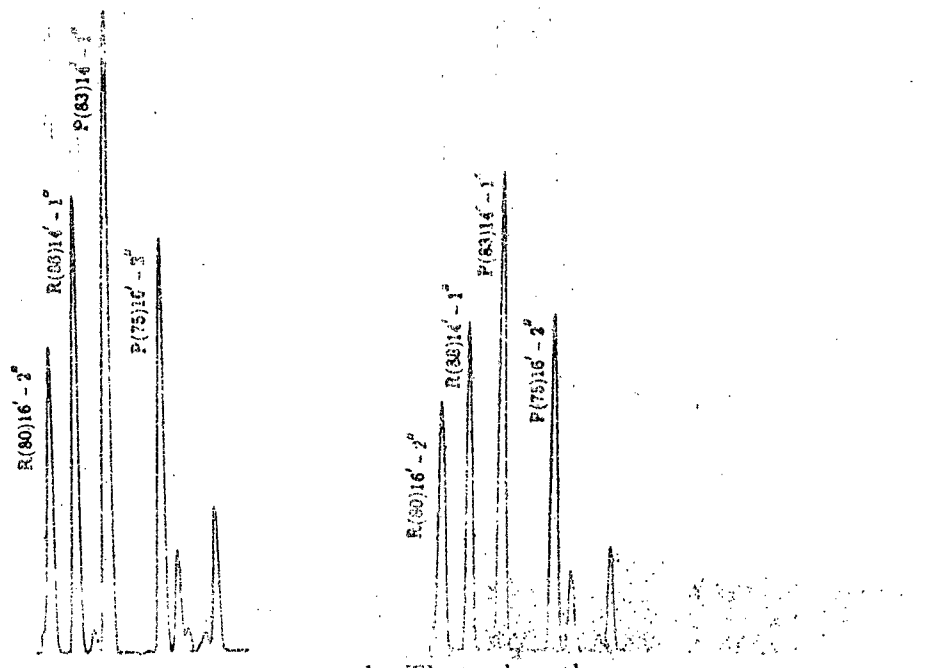

a: Fluorescence from a clean I_2 cell.

b: That when there are impurities in the cell.

Figure 5.17: Fluorescence intensities change due to the impurities in the cell.

intensities are reduced. Booth *et al.*[14] have given a theoretical explanation of this effect. Since the high voltage cell was connected to the pumping system all the times, we could pump out the impurities by keeping the cell at low temperature and opening the valve sc5. Comparing the spectrum before and after the pumping, we could easily observe this effect. Fig. 5.17 shows this effect.

If valve sc5 (refer to Fig. 4.12) had been closed for about an hour, what we observed is the spectrum (b) in Fig. 5.17. Then keeping the cell at -21°C, we opened the sc5 for 10 sec., pumping out the impurities and some I_2 molecules, the spectrum changed to (a) in Fig. 5.17. We can see that the $14' - 1''$ decreased more than $16' - 2''$ lines did. The relative intensities of the lines changed. So if there is a significant amount of impurities in the cell, the predissociation rate we get would be a combination of the two effects –

the electric field induced predissociation and the collision effect. This was taken care of in the experiment by pumping out the cell at about -21°C regularly until no change in relative intensities could be observed.

5.3 Data analysis

5.3.1 Assignment of the spectrum

Frequencies and relative intensities of the fluorescence spectrum of different vibronic bands were calculated using the computer program provided by A. Chanda. During the experiment, a monochrometer was used to monitor the frequency of the laser beam. The pattern and the frequency of the spectrum were compared with the absorption measurements of Gerstenkorn and Luc[15]. The relative intensities and the frequencies were also compared with the calculation. The frequencies agreed usually to within 0.05cm^{-1} and a systematical difference of 0.005cm^{-1} was found. The intensities of the different lines also agreed with the calculation very well, making the line assignment quite straightforward.

5.3.2 Calculations

We have measured electric field induced predissociation for low, medium and high rotational quantum numbers J', from $v'= 4$ to $v'= 9$ vibrational bands. A few measurements for $v'= 12$ and $v'= 16$ bands have been carried on for comparing with the previous results taken by Dalby *et al.*[10]. The predissociation rate constants we got is about 30% higher than the previous value. We do not know the reason for this, but this should has little impact to the assignment of the C potential curve because that only the phases (defined in Section 3.2) of the data points determine the shape of the repulsive potential curve.

Appendix A gives the raw data of these measurements. Appendix B gives all the predissociation rates calculated from the experimental data. For some of them, the

calculated value from the RATIO method and from DIFFERENCE method do not quite agree to each other. There are several reasons for this:

- In the RATIO method, one need not worry about different gains in the different channels. Both I_n and I_e are expressed in a ratio form; it's a very straight forward method. In the DIFFERENCE method, the model 121 and the model 128 lock-in amplifiers may have different gains, and even the model 128 itself may have different gains when it's in DIFFERENCE mode and when it's in SINGLE-CHANNEL mode. The differences between the photo multipliers may also give the contribution to the final result. All these made it difficult to get correct results through this method.

- Eq. 4.47 is equivalent to Eq. 2.14 only when $N_n = E_n$. For some reasons, it happened that D_n was not zero at some frequencies. In this case, we could not make Eq. 4.47 equivalent to Eq. 2.14.

- Difference signal is always noisier, so it is harder to locate the correct baseline of the spectrum.

- Since the scans of N_e, E_e always followed the scans of N_n, E_n, they have the same baseline. Even if the baseline is in error by a small amount, this will not have very big influence on the ratio especially when the predissociation is small. However in the difference method, any error on the baseline would go directly into the calculation of predissociation rate, and the errors are add up. This could possibly change the results a lot.

So we believe the RATIO method is more reliable. We will use the results calculated by this method.

5.4 Rotational quantum number dependence

Table. 5.6 to Table. 5.11 give the predissociation rates constants β calculated by the ratio method as a function of rotational quantum number J'. They are the average of the two β values for the different voltage in the Appendix B. Errors were calculated using the error of N_n, N_e, E_n, E_e listed in Appendix A and follow the Eq. 4.44 to Eq. 4.46. However if this error is smaller than the corresponding error in Appendix B which is obtained by taking the difference of the three calculated βs, the latter is chosen. Fig. 5.18 to Fig. 5.23 are the drawing of the J dependance. The least squared fitting suggested that there is a $J(J+1)$ dependence of the β values from $v' = 4$ to $v' = 9$, where J is the rotational quantum number.

From the least squared fitting of β values from the Table. 5.6 to Table. 5.11, we got their J dependence as:

$$\beta = 0.027(\pm 0.004)J(J+1) + 102(\pm 9) \quad \chi^2 = 5.3 \quad \text{for v} = 4 \tag{5.49}$$

$$\beta = -0.0008(\pm 0.0005)J(J+1) + 43(\pm 1) \quad \chi^2 = 10. \quad \text{for v} = 5 \tag{5.50}$$

$$\beta = 0.0154(\pm 0.0007)J(J+1) + 186(\pm 3) \quad \chi^2 = 4.9 \quad \text{for v} = 6 \tag{5.51}$$

$$\beta = 0.0090(\pm 0.0001)J(J+1) - 8.1(\pm 0.4) \quad \chi^2 = 30. \quad \text{for v} = 7 \tag{5.52}$$

$$\beta = -0.0046(\pm 0.0002)J(J+1) + 121.2(\pm 1.2) \quad \chi^2 = 18. \quad \text{for v} = 8 \tag{5.53}$$

$$\beta = 0.00554(\pm 0.00006)J(J+1) + 84.7(\pm 0.6) \quad \chi^2 = 25. \quad \text{for v} = 9 \tag{5.54}$$

where χ^2 is defined as:

$$\chi^2 = \sum_i \frac{(\beta_i^e - \beta_i^c)^2}{(err.of\beta_i^e)^2} \tag{5.55}$$

5.5 Vibrational quantum number dependence

From the fitting of Fig. 5.18 to Fig. 5.23, one can get the predissociation rate constant β as a function of vibrational quantum number v for a given J. Tab. 5.12 gives this

v′ − v″	p or r	J'	$\beta(cm^2kV^{-2}s^{-1})$
4-4	p	26	99 ± 15
4-4	p	27	100 ± 51
4-4	r	33	125 ± 31
4-4	r	34	142 ± 21
4-4	p	45	175 ± 26
4-4	r	51	158 ± 23
4-4	r	52	215 ± 36
4-4	p	72	267 ± 41
4-4	p	89	286 ± 42

Table 5.6: Predissociation rates for v = 4 vibronic band.

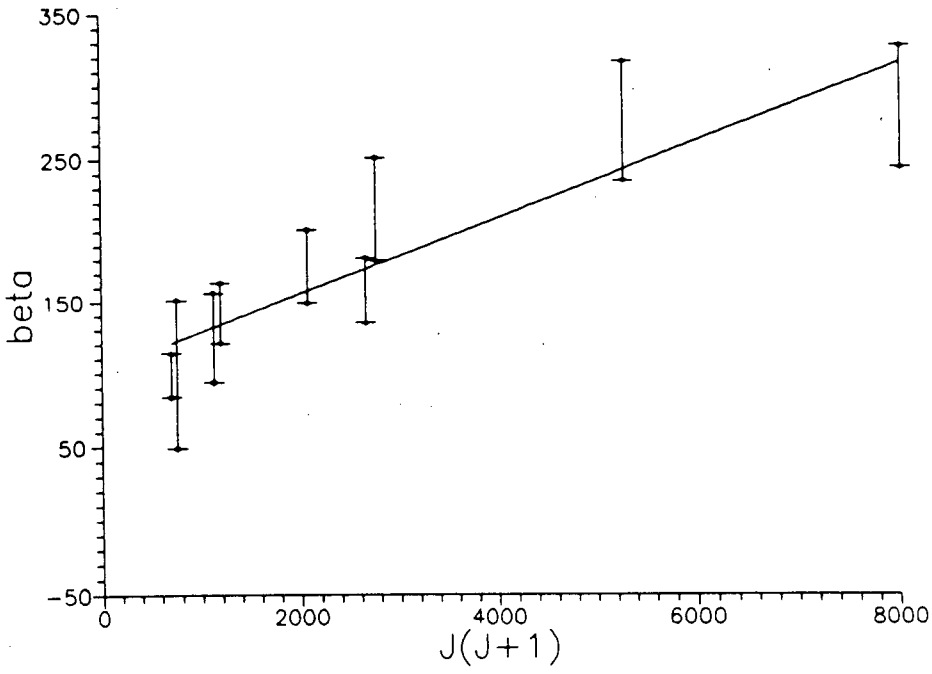

Figure 5.18: J dependence for v = 4 vibronic band.

$v' - v''$	p or r	J'	$\beta(cm^2kV^{-2}s^{-1})$
5-3	p	24	63 ± 9
5-3	p	25	41 ± 6
5-3	r	31	43 ± 7
5-3	p	50	34 ± 8
5-3	r	56	48 ± 7
5-2	p	64	34 ± 5
5-2	r	70	48 ± 7
5-2	p	86	31 ± 5
5-3	p	93	26 ± 13

Table 5.7: Predissociation rates for v = 5 vibronic band.

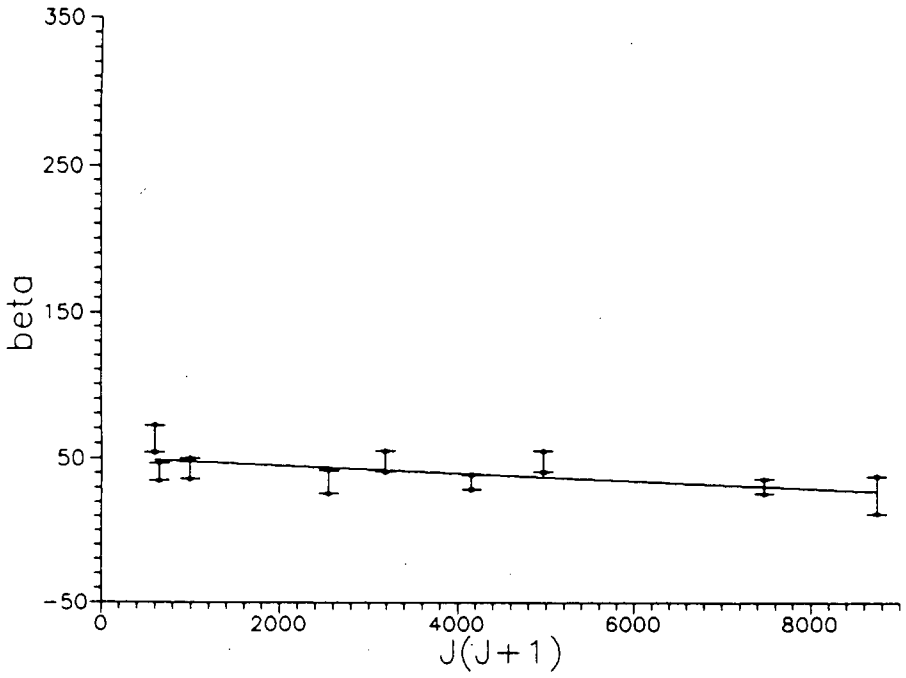

Figure 5.19: J dependence for v = 5 vibronic band.

$v' - v''$	p or r	J'	$\beta(cm^2kV^{-2}s^{-1})$
6-3	p	33	209 ± 14
6-3	r	39	221 ± 15
6-3	p	51	209 ± 15
6-3	r	57	234 ± 16
6-5	r	65	253 ± 51
6-5	r	75	242 ± 29
6-2	p	84	301 ± 21
6-3	p	87	299 ± 23
6-3	r	93	276 ± 17

Table 5.8: Predissociation rates for v = 6 vibronic band.

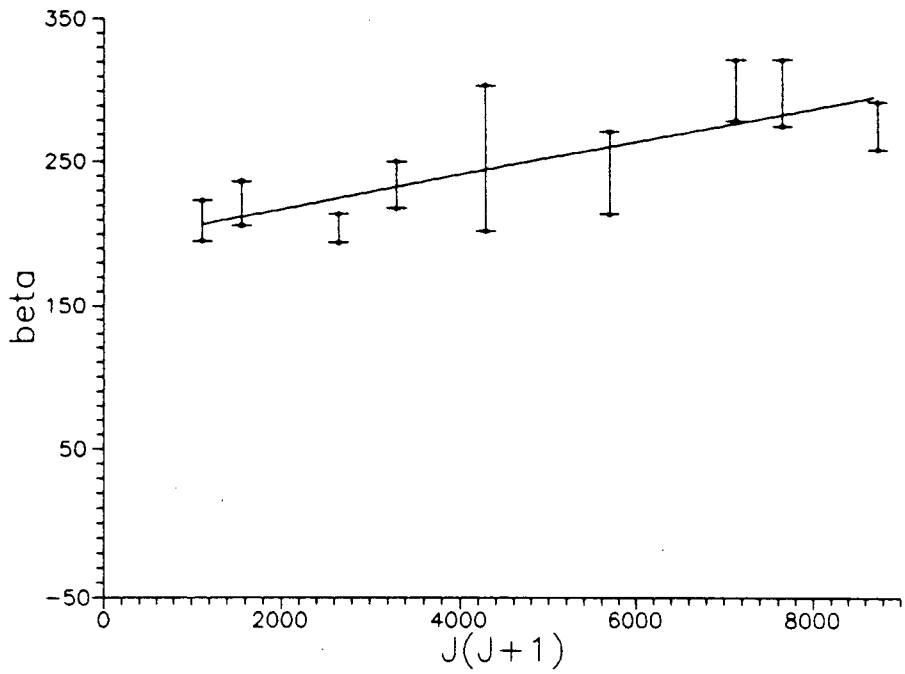

Figure 5.20: J dependence for v = 6 vibronic band.

v′ − v″	p or r	J'	$\beta(cm^2kV^{-2}s^{-1})$
7-3	p	28	11 ± 2
7-3	p	29	4 ± 2
7-3	r	32	6 ± 2
7-3	r	33	9 ± 3
7-3	p	46	10 ± 2
7-3	r	52	17 ± 3
7-4	p	68	26 ± 8
7-4	r	74	26 ± 3
7-3	p	78	36 ± 4
7-3	r	84	50 ± 5
7-3	p	93	82 ± 8

Table 5.9: Predissociation rates for v = 7 vibronic band.

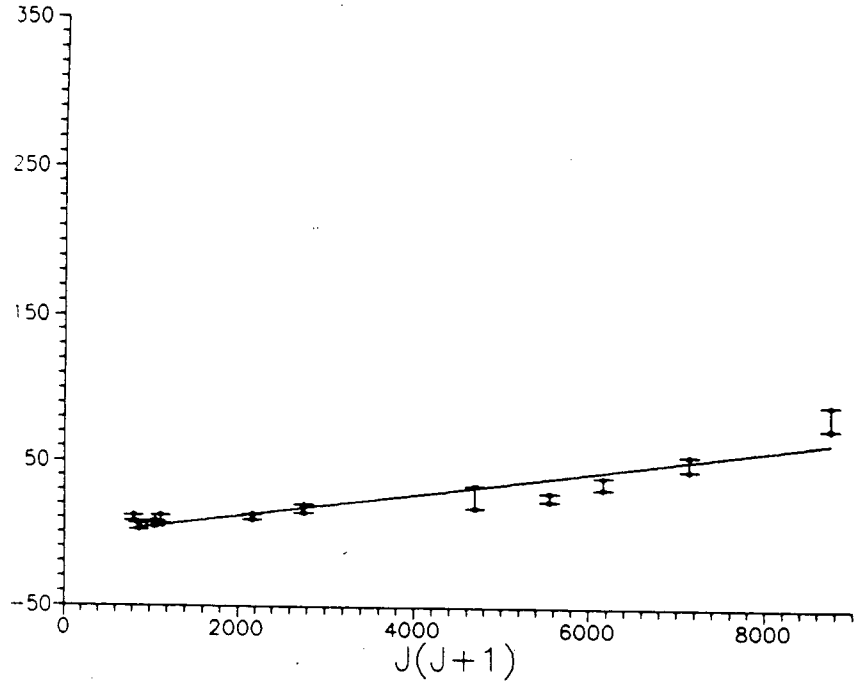

Figure 5.21: J dependence for v = 7 vibronic band.

$v' - v''$	p or r	J'	$\beta(cm^2kV^{-2}s^{-1})$
8-5	p	27	122 ± 11
8-3	p	31	114 ± 9
8-5	r	32	93 ± 7
8-5	r	33	118 ± 9
8-3	r	37	112 ± 9
8-4	p	66	106 ± 8
8-4	r	72	97 ± 7
8-3	p	93	75 ± 6
8-4	p	96	88 ± 7
8-3	r	99	70 ± 5
8-4	r	102	79 ± 5
8-3	p	103	63 ± 5

Table 5.10: Predissociation rates for v = 8 vibronic band.

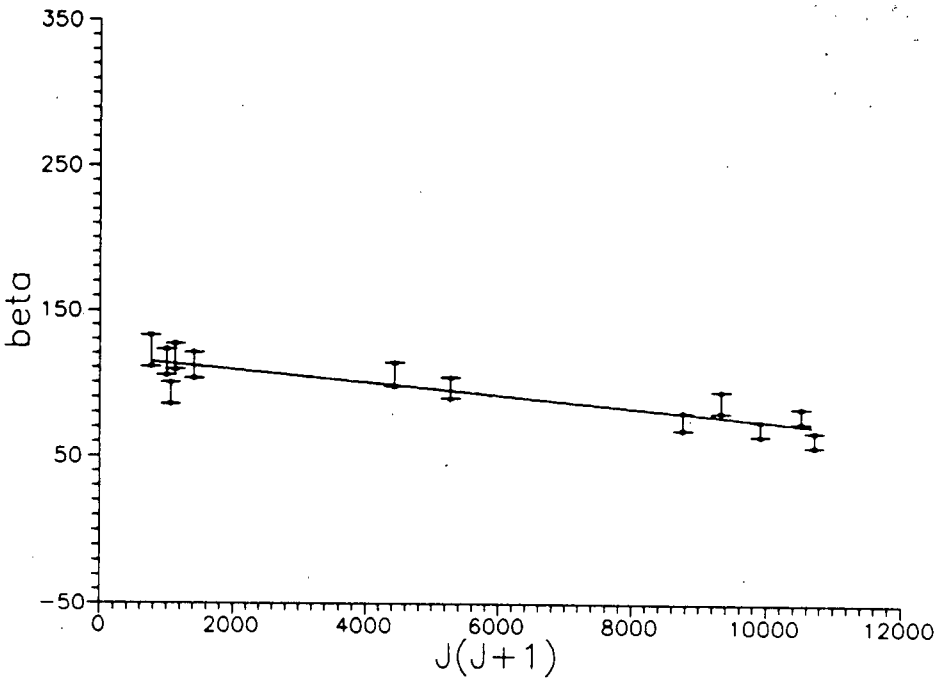

Figure 5.22: J dependence for v = 8 vibronic band.

v′ − v″	p or r	J'	$\beta(cm^2kV^{-2}s^{-1})$
9-4	p	25	88 ± 4
9-4	r	30	82 ± 3
9-4	r	31	95 ± 4
9-4	p	46	103 ± 4
9-4	r	52	106 ± 4
9-4	p	59	119 ± 5
9-4	r	65	122 ± 5
9-4	p	86	132 ± 5
9-4	r	92	145 ± 13
9-4	p	103	144 ± 6
9-3	p	110	155 ± 15
9-4	p	119	166 ± 7

Table 5.11: Predissociation rates for v = 9 vibronic band.

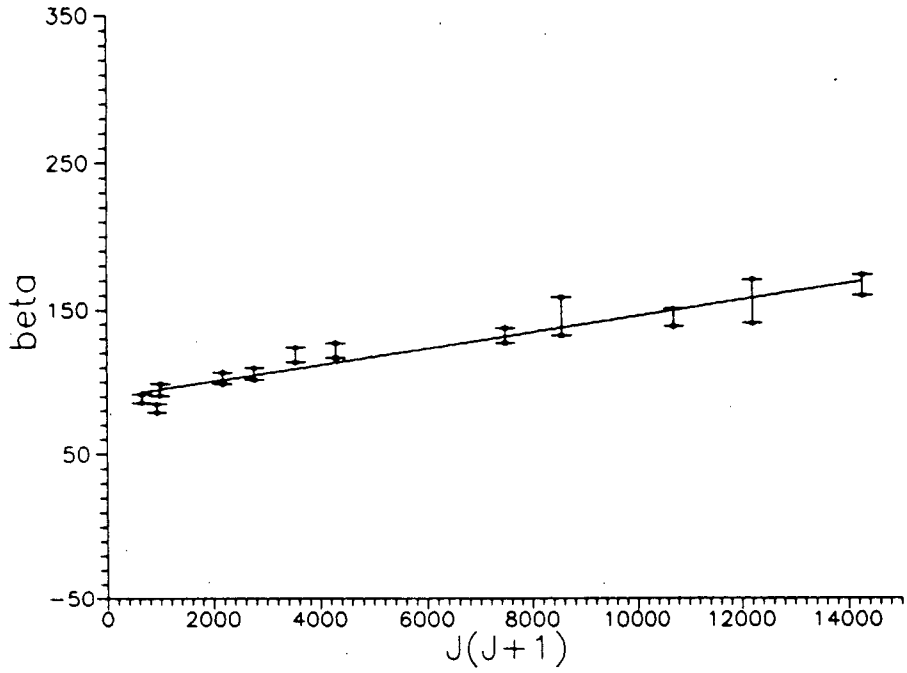

Figure 5.23: J dependence for v = 9 vibronic band.

v	4	5	6	7	8	9
J = 0	108 ± 15	43 ± 4	186 ± 5	-8 ± 1	121 ± 2	85 ± 2
J = 50	180 ± 25	41 ± 5	225 ± 8	15 ± 2	109 ± 3	99 ± 3
J = 100	380 ± 45	35 ± 7	341 ± 15	83 ± 6	75 ± 6	141 ± 5

Table 5.12: v dependence of the predissociation rate.

v	10	11	12	13	14	15	16
J = 0	-2	46	74	17	-4	54	63
J = 50	-2	43	74	21	-4	37	55
J = 100	-2	3	74	50	-4	19	47
v	17	18	19	20	21	22	
J = 0	8	-3	19	35	10	-3	
J = 50	27	-3	4	34	48	26	
J = 100	58	23	-3	22	44	52	

Table 5.13: v dependence of the predissociation rate from Dalby's paper.

dependence for low, medium and high J respectively. Combined with the data from Dalby's paper[10] shown in Tab. 5.13, we have the predissociation rates constants from v = 4 to v = 22. Fig. 5.24, Fig. 5.25 and Fig. 5.24 are the drawings of the predissociation rate constants for $J = 0$, $J = 50$ and $J = 100$ respectively. In these drawings the smooth curves connecting the points are intended as a visual guide only.

From Eq. 3.37 one can see that the curve β against energy should be a sine squared form with the amplitude modulation. Taking out the amplitude modulation from Fig. 5.24 etc., one can get a sine square curve out of which one can get the phase for each data point. This phase Φ can be expressed as a function of energy ε. Tab. 5.14 and Fig. 5.27 gives this relationship. The least square fitting gives the expression of this as:

$$\Phi = -9.689 \times 10^{-7}\varepsilon^2 + 0.01152\varepsilon + 1.989 \tag{5.56}$$

This $\Phi(\varepsilon)$ then can be used to calculate the C potential curve as described in Eq. 3.38,

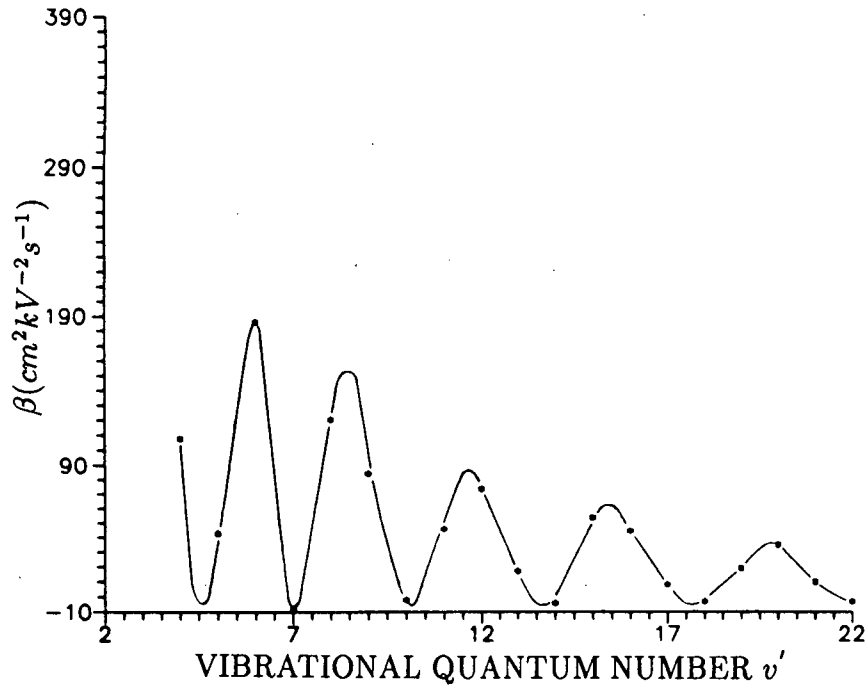

Figure 5.24: The measured predissociation rate constants β for $J = 0$ as a function of vibrational quantum number of the B state of molecular iodine.

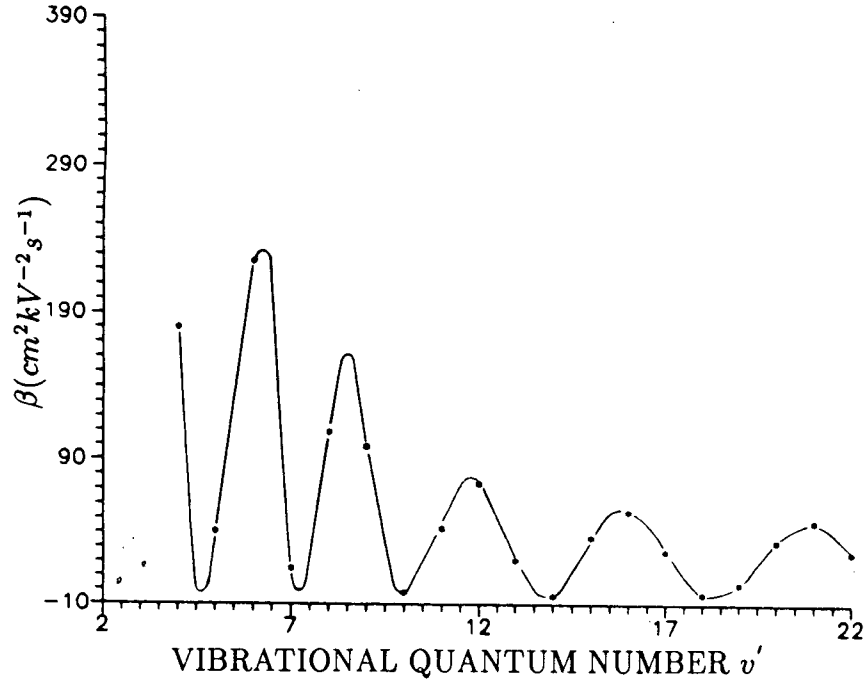

Figure 5.25: The measured predissociation rate constants β for $J = 50$ as a function of vibrational quantum number of the B state of molecular iodine.

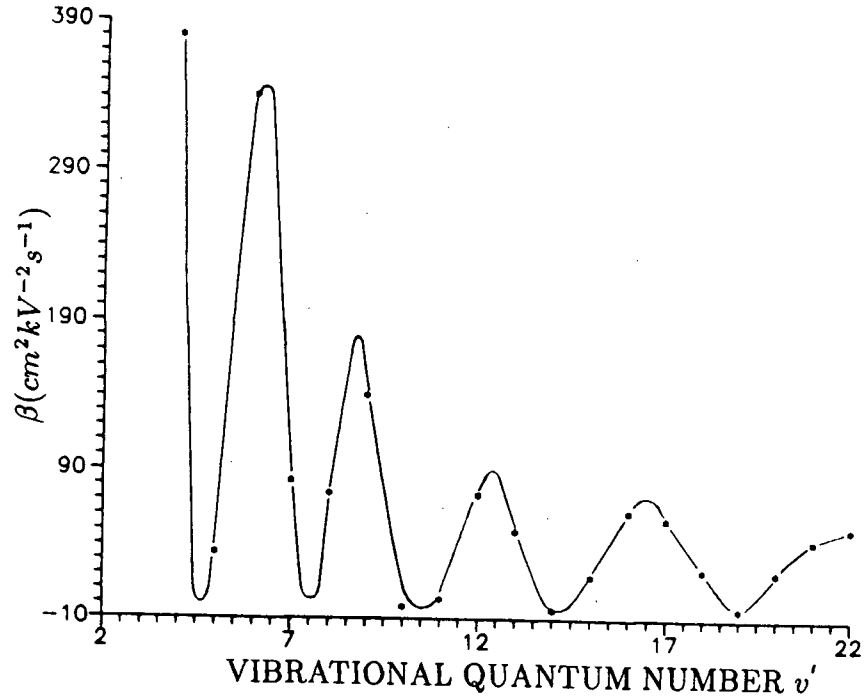

Figure 5.26: The measured predissociation rate constants β for $J = 100$ as a function of vibrational quantum number of the B state of molecular iodine.

but this method failed in our case because a potential curve which is not a single-valued function of internuclear distance r was derived. In the curve as the energy decreases the internuclear distance increases then decreases. The possibility that the C potential curve might have huge slope has caused concern about the validity of some approximation made in semiclassical theory. To avoid these, we tried to use numerical method to solve the problem.

v'	$\varepsilon\ cm^{-1}$	phase Φ
4	549.97	7.77
5	667.88	9.14
6	784.18	10.37
7	898.83	11.78
8	1011.82	12.86
9	1123.17	13.97
10	1232.80	14.92
11	1340.72	15.77
12	1446.90	16.50
13	1551.33	17.61
14	1653.97	18.06
15	1754.80	19.17
16	1853.81	19.88
17	1950.96	20.81
18	2046.22	21.21
19	2139.61	22.02
20	2231.06	22.78
21	2320.58	23.78
22	2408.13	24.34

Table 5.14: The phase of the electric field induced predissociation rate constant as a function of energy for J = 0.

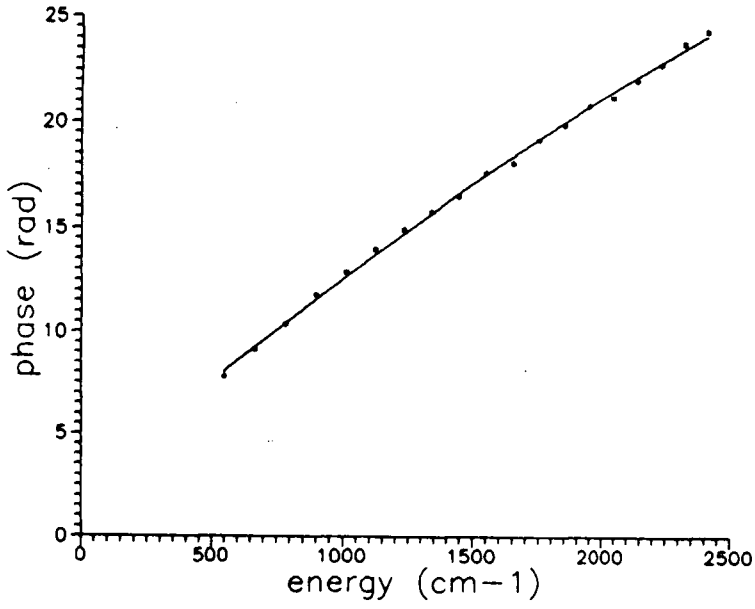

Figure 5.27: The phase (defined in Section 3.2) of the electric field induced predissociation rate constant as a function of energy for J = 0.

Chapter 6

Numerical Solution

6.1 Formulas and constants

We want to locate where the crossing of the two potential curves is and to determine the slope of the C curve. So for the small vibrational quantum numbers, we suppose the C curve is a straight line. By quantum mechanics theory, the wave function of a straight line potential curve has the form(See Appendix C):

$$\chi(\eta) = A\Upsilon(-\eta) \tag{6.57}$$

where η is defined as:

$$\eta = \left(r + \frac{\varepsilon - B}{F}\right)\left(\frac{2mF}{\hbar^2}\right)^{\frac{1}{3}} \tag{6.58}$$

$\Upsilon(\eta)$ is called the *Airy function*; A is the normalization factor; r is the internuclear distance; ε is the energy; F is the absolute value of the slope of the potential straight line; B equals to $F \times b$, while b is the intercept of the potential straight line on the r axis. Normalize the wavefunction to Delta function of energy by the equation:

$$\int_{-\infty}^{\infty} \chi(\eta)\chi(\eta')\mathrm{d}r = \delta(\varepsilon' - \varepsilon). \tag{6.59}$$

We can find the normalization coefficient is[3, page 75]

$$A = \frac{(2m)^{1/3}}{\pi^{1/2}F^{1/6}\hbar^{2/3}} \tag{6.60}$$

where m is the reduced mass of iodine molecule.

Take m equal to 1.0545×10^{-25} Kg. Then we get

$$\chi(r) = \frac{1.9695 \times 10^{16}}{F^{\frac{1}{6}}} \Upsilon \left[-1.5563 F^{\frac{1}{3}} (r - b + \frac{\varepsilon}{F}) \right] \tag{6.61}$$

where F is in $\frac{cm^{-1}}{\mathring{A}}$; ε is in cm^{-1}; r and b are in $\mathring{A}$. The unit of χ is $\frac{S}{Kg^{1/2}m^{3/2}}$.

The Airy function can be numerically calculated by an ascending series:

$$\Upsilon(\eta) = 0.35503 \sum_0^\infty 3^k \left(\frac{1}{3}\right)_k \frac{\eta^{3k}}{(3k)!} + 0.25882 \sum_0^\infty 3^k \left(\frac{2}{3}\right)_k \frac{\eta^{3k+1}}{(3k+1)!} \tag{6.62}$$

where

$$\begin{aligned} \left(\alpha + \frac{1}{3}\right)_0 &= 1 \\ \left(\alpha + \frac{1}{3}\right)_k &= (3\alpha + 1)(3\alpha + 4) \cdots (3\alpha + 3k - 2) \\ &\qquad (\alpha \text{ arbitrary}; \quad k = 1, 2, 3, \ldots) \end{aligned}$$

When η is large, we can simply use the semiclassical expression[3, page 345]:

$$\chi(r) = \sqrt{\frac{2}{\pi \hbar v}} cos \left[\frac{1}{\hbar} \int_a^r p(r') \mathrm{d}r' - \frac{1}{4}\pi \right] \tag{6.63}$$

This is also normalized by delta function of momentum. A factor of $\sqrt{\pi}$ has to be added to Eq. 6.63 to be consistent with Eq. 6.61. (The Eq. 24.6 and the Eq. 24.4 in page 75 of reference [3] also differ by factor of $\sqrt{\pi}$.) With

$$p = mv = \sqrt{2m(\varepsilon - U(r))}, \tag{6.64}$$

Eq: 6.63 becomes

$$\chi(r) = \frac{9.94814 \times 10^{15}}{(E - U(r))^{\frac{1}{4}}} \cos \left[1.9408 \int_a^r \sqrt{E - U(r')} \mathrm{d}r' - \frac{\pi}{4} \right], \tag{6.65}$$

where E and U are in cm^{-1}; r is in $\mathring{A}$.

The B state wavefunction can be calculated using semiclassical expression:

$$\chi(r) = \sqrt{\frac{2\omega}{\pi v(r)}} \cos \left[\frac{1}{\hbar} \int_a^r p(r') \mathrm{d}r' - \frac{\pi}{4} \right] \quad \text{for } E > U(r) \tag{6.66}$$

$$\chi(r) = \sqrt{\frac{\omega}{2\pi|v(r)|}} \exp\left[-\frac{1}{\hbar}\left|\int_a^r p(r')\mathrm{d}r'\right|\right] \quad \text{for } E < U(r) \tag{6.67}$$

These are normalized by

$$\int_a^b |\chi|^2 \mathrm{d}r = 1. \tag{6.68}$$

Since the wavefunction in the classical unacceptable region would give very little contribution to the integral, the integral limitation was taken from a to b instead of from 0 to ∞, where a and b are left and right turning points. The unit of χ is $1/\sqrt{m}$. The classical oscillation frequency ω can be calculated according to

$$\omega_v = \frac{E_v - E_{v-1}}{\hbar}, \tag{6.69}$$

where v is vibrational quantum number. Working out all the constants for the Eq: 6.66, we have

$$\chi(r) = 78600.5 \times \sqrt{E_v - E_{v-1}} \times (E_v - U(r))^{-\frac{1}{4}} \cos\left[1.9408 \times \int_a^r \sqrt{E_v - U(r')}\mathrm{d}r' - \frac{\pi}{4}\right]. \tag{6.70}$$

The constants for Eq: 6.67 are similar. The semiclassical expression is only good when the atoms are far from turning points. Eq: 6.66 and Eq: 6.67 should joint smoothly at the turning points, but they both tend to infinity at the turning points. In these small neighborhoods of turning points, we have to change empirically the calculated data to join the two curves. To test this change, we did the integral according the Eq: 6.68 and got 1.03 ± 0.01 for all the vibrational levels involved. This means the change is reasonable within 3% error. To correct this 3% error, we used these data to re-normalize the wave function. The actual constants used are: 1.0467, 1.0395, 1.0405, 1.0377, 1.0292 and 1.0325 for vibrational level 4, 5, 6, 7, 8, and 9 respectively.

Now we have got both B state and the C state wave functions numerically. We generated a computer program to multiply the two wavefunction and do the integral

from $-\infty$ to $+\infty$ according to the definition Eq. 3.15. We give a rough estimation of the amplitude of the dipole moment μ as:

$$\mu = ez = 1.6 \times 10^{-19}(C) \times 10^{-11}(m) = 1.6 \times 10^{-21}(Cm). \tag{6.71}$$

After the constants are put into Eq. 3.15, it becomes:

$$\beta = 5.9545 \times 10^{-36} \left| \int_{-\infty}^{+\infty} \chi_B \chi_C \mathrm{d}r \right|^2 \tag{6.72}$$

Where dr is in the unit of $\mathring{A}$. There are two parameters varied during the numerical calculation. One is the location of crossing point, the other is the slope of the C potential curve. We scanned the intersection from left turning point to the right turning point of $v = 4$ vibrational state by every 0.002 $\mathring{A}$. The slope of the C potential curve was changed from $10^3 cm^{-1}/\mathring{A}$ to $10^4 cm^{-1}/\mathring{A}$ by every $0.5 \times 10^3 cm^{-1}/\mathring{A}$, then from $10^4 cm^{-1}/\mathring{A}$ to $10^5 cm^{-1}/\mathring{A}$ by every $0.5 \times 10^4 cm^{-1}/\mathring{A}$, and finally from $10^5 cm^{-1}/\mathring{A}$ to $10^6 cm^{-1}/\mathring{A}$ by every $0.5 \times 10^5 cm^{-1}/\mathring{A}$. We calculated β value for many possible positions of the C potential curve. Since Eq: 6.71 only gives a rough estimate of dipole moment μ, a constant factor is left out in the expression 6.72. In order to evaluate the calculation, a constant K has to be worked out to get the smallest $least - squared - difference$ value. The lsd value is defined as

$$lsd = \frac{\sum_{i=4}^{9}(\beta_i^e - K \times \beta_i^c)^2}{\sum_{i=4}^{9}(\text{err. of } \beta_i^e)^2}, \tag{6.73}$$

where β^e are experimental results and β^c are calculated data. A good fit should give lsd value as about 1. The denominator is denoted as ERR which is a constant. It is 450 for $j = 0$. Differentiate Eq: 6.73, we can get the expression of K as

$$K = \frac{\sum_{i=4}^{9} \beta_i^e \times \beta_i^c}{\sum_{i=4}^{9}(\beta_i^c)^2}. \tag{6.74}$$

slope($\times 10^{-4} cm^{-1}/\mathring{A}$)	lsd						
5.00	41.	31.	25.	20.	10.	4.1	3.3
6.00	29.	17.	12.	7.7	2.1	2.1	8.9
7.00	21.	11.	6.6	3.7	1.6	5.7	16.
8.00	16.	7.1	4.0	2.0	2.4	9.7	24.
9.00	9.3	3.0	1.4	1.0	4.3	13.	29.
10.00	8.1	2.0	0.8	1.3	7.0	19.	36.
15.00	3.8	3.0	4.5	7.7	19.	37.	58.
20.00	3.0	5.0	7.8	12.	24.	42.	62.
25.00	3.0	6.9	11.	17.	32.	50.	71.
30.00	3.6	8.1	13.	19.	35.	53.	73.
35.00	4.3	10.	15.	21.	36.	55.	77.
40.00	3.9	10.	14.	20.	36.	57.	78.
45.00	5.2	12.	16.	23.	40.	60.	80.
50.00	5.3	13.	18.	25.	43.	63.	82.
intercept($\mathring{A}$)	3.061	3.063	3.064	3.065	3.067	3.069	3.071

Table 6.15: Calculated predissociation rate constants by quantum mechanic method for J = 0.

6.2 Numerical result

Tab. 6.15 gives calculated *lsd* value in the near neighborhood of the crossing point(where *lsd* value are among the smallest).

The global minimum lsd value is 0.76. It happens when the slope of the C potential curve is $9.77 \times 10^4 cm^{-1}/\mathring{A}$ and the crossing point with r axis is R = $3.064\mathring{A}$. All the local minimums which are not shown in the Table 6.15 are bigger than 3. Fig. 6.28 gives the B state wavefunction for $v' = 5$ vibrational state and the C state wavefunction at above slope and intersection.

The calculated predissociation rate constant β at the above slope and intercept is shown in Table 6.16. In the third column of the Table 6.16 are the calculated r_C values of the C potencial curve (for J = 0) at which energy (second column) applied. Also shown

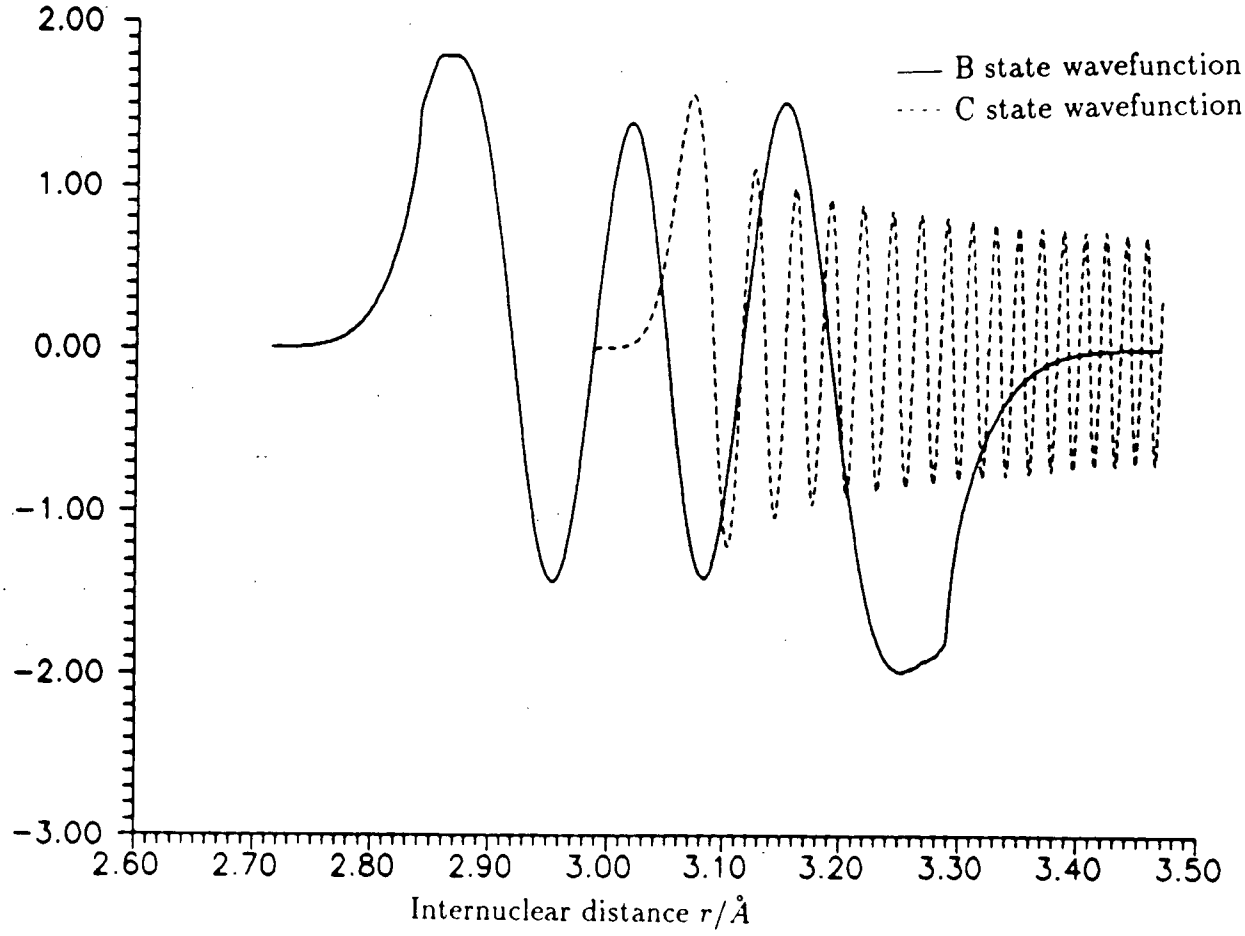

Figure 6.28: B state wave function for $v' = 5$, $E' = 667.88\text{cm}^{-1}$ and C state wavefunction for slope $= 9.77 \times 10^4\text{cm}^{-1}/\AA$, intercept $= 3.064\ \AA$ and $E' = 667.88\text{cm}^{-1}$.

v	ε (cm^{-1})	rc ($\AA$)	β^e	β^c
4	549.97	3.0585	102±20	122
5	667.88	3.0573	43±4	47.5
6	784.18	3.0562	186±5	177
7	898.83	3.0550	-8±1	3.3
8	1011.82	3.0534	121±2	117
9	1123.17	3.0528	85±2	86.3

Table 6.16: Calculated predissociation rate constants for $J = 0(lsd = 0.76, \mathrm{K} = 3.149)$.

in the table is the experimental data for the same vibrational and rotational quantum numbers for comparison. The errors of the β^e in Table 6.16 are estimated from the Fig. 5.18 to Fig. 5.23. They are not same with computer calculated errors shown in Eq.5.48 to Eq.5.53.

6.3 Fitting for higher J value

For the B state of molecular iodine, the effective potential curve for a given rotational quantum number J is related to the potential curve of $J = 0$ by[3, pages 314-316]:

$$U_J(r)(cm^{-1}) = U_{J=0}(r)(cm^{-1}) + \frac{h}{8\pi^2 mc}(\AA^2 cm^{-1})\frac{J(J+1)}{r^2} \tag{6.75}$$

Taking $m = 1.0545 \times 10^{-25} Kg$ as before, we got the effective potential curves for both $J = 50$ and $J = 100$ of the vibrational levels 4 to 9.

The energy corresponding to a given rotational level can also be written as:

$$E_J = E_{J=0} + B_v J(J+1) - D_v J^2(J+1)^2 \tag{6.76}$$

Where B_v is called *rotational constant* in the vibrational state v, which is actually the average of the term $B(R) = \frac{\hbar^2}{2mr^2}$ over r in this vibrational state. D_v is the quadratic centrifugal distortion constant. Using the B_v and D_v values given by Gerstenkorn and

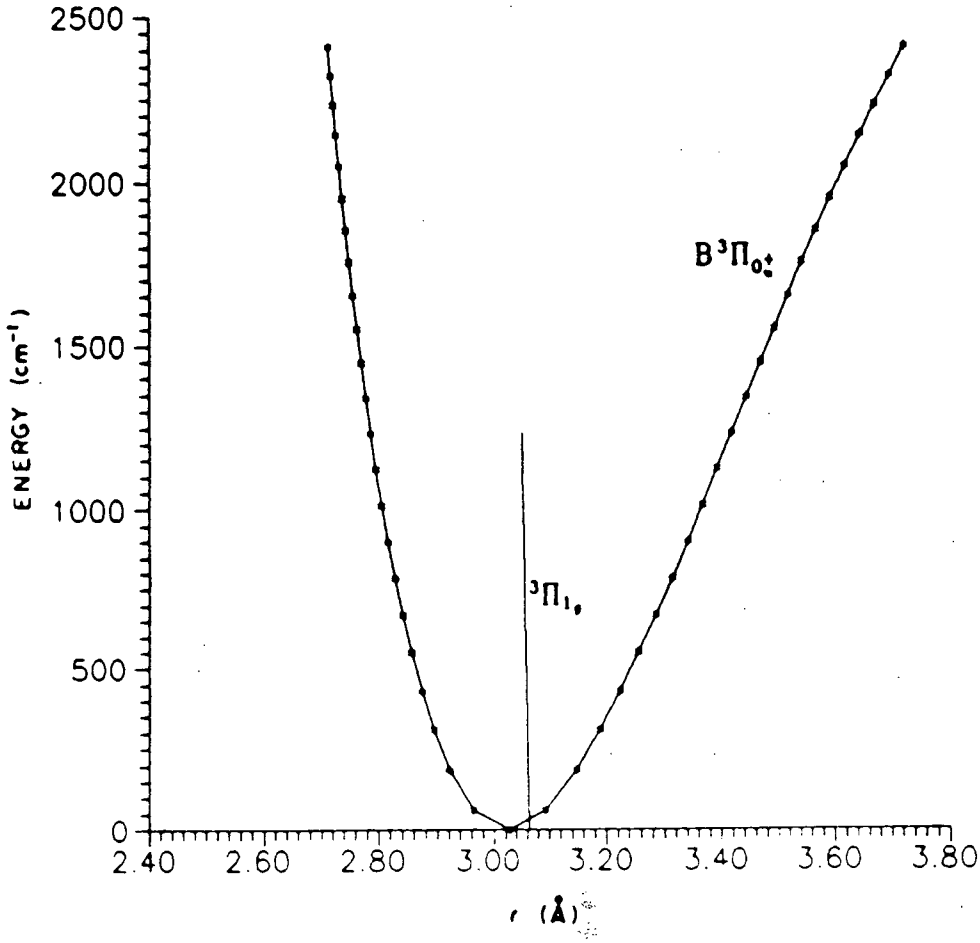

Figure 6.29: Revised $^3\Pi_{1_g}$ state potential curve.

v	turning points of J=0		turning points of J=50		turning points of J=100	
	R_{min} Å	R_{max} Å	R_{min} Å	R_{max} Å	R_{min} Å	R_{max} Å
4	2.85696	3.25645	2.85842	3.25862	2.86226	3.26548
5	2.84203	3.28614	2.84348	3.28839	2.84735	3.29599
6	2.82880	3.31436	2.83024	3.31696	2.83414	3.32453
7	2.81690	3.34153	2.81838	3.34394	2.82225	3.35183
8	2.80606	3.36794	2.80749	3.37044	2.81150	3.37863
9	2.79616	3.39350	2.79759	3.39609	2.80177	3.40426

Table 6.17: Classical turning points for J = 0, 50, 100 effective potential curves.

Luc[23], the energy of $J = 50$ and $J = 100$ levels of $v = 4$ to 9 were also calculated. With these energy values and the effective potential curves calculated by Eq: 6.75, we calculated classical turning points of these potential curves for the different vibrational levels. Table 6.17 shows the result. The turning points of $J = 0$ potential curve shown in this table comes from Barrow and Yee's paper[12].

Using the same procedure we used to $J = 0$ potential curve, we calculated B state wavefunctions for $J = 50$ and $J = 100$ of $v = 4$ to 9 and then the slope and the intercept of the C state potential curve. The results agree with $J = 0$'s result very well except for the data of $J = 100$, $v = 9$ which is ignored in the table 6.19. Table 6.18 and Table 6.19 show the results.

For J = 0, The calculated β values agree with experimental values very well for all the vibrational level (refer to Table 6.16). For J = 50 (6.18), we got good agreement only for low v. And we have to ignore calculated β for $v = 9$ for J = 100 in order to get reasonable small lsd value. This suggestes that C potencial curve has a bigger curvature for higher J. Since we suppose that C potencial curve is a straight line, this method is less appliable for higher J.

If we take the region with $lsd < 1.0$ as acceptable, we can work out the error of the

v	ε (cm^{-1})	rc ($\AA$)	β^e	β^c
4	622.10	3.0594	180±25	171
5	739.60	3.0582	41±5	37.8
6	855.47	3.0570	225±8	219
7	969.69	3.0558	15±2	11.0
8	1082.25	3.0547	109±3	119
9	1193.15	3.0535	99±3	115

Table 6.18: Calculated predissociation rate constants for $J = 50(lsd = 0.68, \mathrm{K} = 3.755)$.

v	ε (cm^{-1})	rc ($\AA$)	β^e	β^c
4	835.15	3.0576	380±45	373
5	951.40	3.0563	35±7	4.47
6	1066.02	3.0550	341±15	342
7	1233.05	3.0531	83±6	86.4
8	1290.21	3.0525	75±6	96.9
9	1399.78	3.0513	141±5	

Table 6.19: Calculated predissociation rate constants for $J = 100(lsd = 0.64, \mathrm{K} = 5.586)$.

result(refer to Table 6.15). The $^3\Pi_{1_g}$ state potential curves of $J = 0$, $J = 50$ and $J = 100$ all intersect the corresponding $\mathrm{B}\,^3\Pi_{0_u^+}$ state potential curves at $R = 3.064 \pm 0.001\AA$ with the slope $9.8(\pm 0.3) \times 10^4, \mathrm{cm}^{-1}/\AA$, $9.8(\pm 0.3) \times 10^4, \mathrm{cm}^{-1}/\AA$ and $8.9(\pm 0.4) \times 10^4, \mathrm{cm}^{-1}/\AA$ respectively.

6.4 Conclusion

In this paper, we have presented a detailed research on the electric field induced predissociation of molecular I_2 . The induced predissociation rate constant of $v = 4$ to $v = 9$ was

measured in a electric field as high as 133 kV/cm. Combining with the previous work by Dalby *et al.*, we have obtained the most completed data of induced predissociation of I_2 . A detailed table and a drawing (Fig. 6.29) about the revised $^3\Pi_{1_g}$ potential curve has be given. Compare to the result previously given by Dalby *et al.*[10], the slope of the C potential obtained through this work is about factor of 5 smaller and the interception shifted to right by $0.08\mathring{A}$.

Appendix A

Experimental Data

Tab. A.20 give the parameters used to calculate the natural predissociation rate; these data are from Vigué's paper[16]. According to Eq: 2.11, Eq: 1.2 and Eq: 1.3, the total radiative decay rate Γ_T is calculated by

$$\Gamma_T = \Gamma_R + C_v^2 J(J+1) + 4.7a_v^2 \qquad \text{for even J} \tag{A.77}$$

$$\Gamma_T = \Gamma_R + C_v^2 J(J+1) + 6.8a_v^2 \qquad \text{for odd J} \tag{A.78}$$

where Γ_C is taken as zero due to the low pressure in the cell. The calculated Γ_T for all the transitions is given in appendix B.

Starting from page 63 in this appendix lists all the raw data from our experiment. In the lists v', v'' is the upper and lower vibrational quantum number respectively; PR means P or R branch; J is rotational quantum number; E is electric field strength in the unit of kV/cm; $N0$ and $E0$ are the peak fluorescence intensity of given rotational transitions in the field free region and field region respectively when electric field is not applied. $D0$ is the difference of the above two transitions measured electronically. Con is the converting factor defined in Eq. 4.48 and only be used in DIFFERENCE method. Ni and Ei (i = 1, 2, 3) are the peak fluorescence intensity of given rotational transitions in the field free region and field region respectively when electric field is applied. Di (i = 1, 2, 3) is the difference of the above two transitions measured electronically. The numbers in the brackets are the errors. These data were used in the program *data.c* to calculate the predissociation rate constants. Here we give one example of calculation.

v	$C_v^2\ (\frac{1}{s})$	$a_v^2\ (\frac{1}{s})$	$\Gamma_R\ (\frac{1}{s})$
4	292.	339000.	908000.
5	314.	363000.	897000.
6	303.	350000.	884000.
7	287.	324000.	872000.
8	187.	232000.	860000.
9	141.	146000.	847000.
10	95.	110000.	833000.
11	51.	40000.	819000.
12	21.	16000.	806000.

Table A.20: Constants C_v^2, a_v^2 and Γ_R used in the calculation of predissociation rate constants β.

For the first group of data in the list, the transition is $10' - 4''$ $r51$, taking constants from Tab. A.20 and using Eq. A.78 we have

$$\Gamma_T = 833000. + 95 \times 51 \times (51+1) + 6.8 \times 110000 = 1.83 \times 10^6 \tag{A.79}$$

For RATIO method, using Eq: 4.47 we have

$$\beta_1 = \frac{\Gamma_T}{E^2} \times \frac{\frac{N1}{N0} - \frac{E1}{E0}}{\frac{E1}{E0}} = \frac{1.83 \times 10^6}{138^2} \times \frac{\frac{102}{97} - \frac{112}{110}}{\frac{112}{110}} = 3.2 \tag{A.80}$$

β_2 is calculated similarly using $N2$, $E2$, $N0$, $E0$. In total 5 β can be obtained using 5 sets of data for a given transition. The average of these 5 β was used as the electric field induced predissociation rate constant. For DIFFERENCE method, β was calculated by

$$\beta_1 = \frac{\Gamma_T}{E^2} \times \frac{D1}{E1 \times Con} = \frac{1.83 \times 10^6}{138^2} \times \frac{22 \times 1.24}{112 \times 2.024} = 11. \tag{A.81}$$

Where constant 1.24 corrects the gain difference of the two lock-in amplifiers and is same for all data. The constant 2.024, read from data listed below, corrects the gain difference due to different setting related to two lock-in amplifiers and will change among different group of data. We also have 5 different β for a given transition, but these data were not used and the reason was discussed in Chapter 5.

v'	v"	J	E (kV/cm)	N0 (1.)	E0 (2.)	D0 (3.)	N1 (1.)	E1 (2.)	D1 (3.)	N2 (1.)	E2 (2.)	D2 (3.)	N3 (1.)	E3 (2.)	D3 (3.)	Cov. (0.003)
10	4	r51	138.	97.	110.	0.	101.5	111.5	21.5	101.5	109.	23.	96.	102.	25.	2.024
9	3	p110	138.	38.5	44.	0.	39.5	24.5	41.	38.	22.	44.	38.	23.5	41.	2.024
8	3	r37	138.	128.	159.5	29.	135.	94.	119.5	136.	96.	115.	132.	94.	112.	2.024
8	3	p31	138.	109.5	138.	29.	116.	80.	104.	116.	79.5	106.	114.	78.5	102.	2.024
10	4	p45	138.	93.5	106.	0.	101.	109.	20.	104.	112.5	20.	99.	106.	26.	2.024
10	4	r51	96.9	97.	110.	0.	95.	102.5	11.	89.	97.	9.				2.024
9	3	p110	96.9	38.5	44.	0.	37.	30.	23.	35.5	27.	24.5				2.024
8	3	r37	96.9	128.	159.5	29.	131.	115.	64.	123.	108.	59.				2.024
8	3	p31	96.9	109.5	138.	29.	109.5	94.5	58.	94.	84.5	50.				2.024
10	4	p45	96.9	93.5	106.	0.	100.	107.	10.	90.	97.	9.				2.024

v'	v"	J	E (kV)	N0 (1.)	E0 (1.)	D0 (3.)	N1 (1.)	E1 (1.)	D1 (3.)	N2 (1.)	E2 (1.)	D2 (3.)	N3 (1.)	E3 (1.)	D3 (3.)	Cov. (0.003)
8	3	r99	138.	121.	133.	0.	111.	95.	73.	125.5	107.5	83.	106.	88.	77.	4.048
10	4	p98	138.	93.	87.	42.	91.	68.	87.	99.5	74.	92.	77.5	60.	70.	4.048
8	3	p93	138.	162.5	178.5	0.	165.5	133	128.5	167.5	135.	129.	130.5	104.	104.	4.048
6	2	p84	138.	62.5	65.	15.	70.	34.	108.	61.5	30.	97.	52.5	25.5	82.	4.048
8	3	r99	96.9	121.	133.	0.	121.5	114.	56.	121.	115.	48.				4.048
10	4	p98	96.9	93.	87.	42.	90.	76.5	61.	91.	73.5	69.				4.048
8	3	p93	96.9	162.5	178.5	0.	152.	143.	68.	141.5	132.5	61.				4.048
6	2	p84	96.9	62.5	65.	15.	63.5	40.	76.	59.	37.5	68.5				4.048

v'	v"	J	E (kV)	N0 (1.)	E0 (1.)	D0 (1.)	N1 (1.)	E1 (1.)	D1 (1.)	N2 (1.)	E2 (1.)	D2 (1.)	N3 (1.)	E3 (1.)	D3 (1.)	Cov. (0.004)
8	3	p103	138.	98.	120.	-11.	92.	88.	15.	85.5	82.	14.	100.	97.5	16.	1.007
9	4	r 31	138.	211.	220.5	15.	197.	108.	114.	177.	96.5	103.	218.	120.	126.	1.007
9	4	p 25	138.	186.	193.	15.	174.	97.	102.	153.5	86.	87.5	187.	105.	107.	1.007
10	4	p107	138.	105.	114.	4.	102.	75.	40.	81.	60.	31.	105.	80.	41.	1.007
9	4	r 30	138.	199.	203.	20.	189.5	101.	114.5	157.	83.5	95.5	197.	106.	118.	1.007
8	3	p103	96.9	98.	120.	-11.	101.	108.5	5.	99.5	107.	4.				1.007
9	4	r 31	96.9	211.	220.5	15.	219.5	155.	92.	216.	153.5	89.5				1.007
9	4	p 25	96.9	186.	193.	15.	189.5	136.	78.	189.5	134.	78.				1.007
10	4	p107	96.9	105.	114.	4.	107.	91.5	29.	107.	92.	27.				1.007
9	4	r 30	96.9	199.	203.	20.	200.	138.	88.	198.	137.	85.				1.007
7	3	p 29	138.	91.5	111.	-9.	96.	112.	11.	95.	111.	13.	85.	101.	-11.	1.007

7	3	r	33	138.	105.5	130.	-11.	114.	130.5	12.	110.5	129.	12.	100.	118.	-11.	1.007
9	4	r	52	138.	130.	138.	7.	140.	74.5	81.	136.5	71.	77.	127.	69.	75.	1.007
9	4	p	46	138.	132.	140.	7.	141.5	73.	83.	139.	73.	83.	129.	68.5	78.	1.007
7	3	p	28	138.	93.	112.	-8.5	99.	111.	13.	99.	110.5	13.	90.	101.	-10.	1.007
7	3	r	32	138.	104.	125.5	-10.	108.	126.5	7.	107.	123.	6.	100.	116.5	-6.	1.007
7	3	p	29	96.9	91.5	111.	-9.	93.5	113.5	-10.	93.	112.	-11.				1.007
7	3	r	33	96.9	105.5	130.	-11.	107.5	130.5	-10.	110.	132.	-12.				1.007
9	4	r	52	96.9	130.	138.	7.	133.	91.5	59.	131.5	90.	57.				1.007
9	4	p	46	96.9	132.	140.	7.	130.	90.	57.	142.5	97.	63.				1.007
7	3	p	28	96.9	93.	112.	-8.5	91.	106.	-9.	100.	115.	-10.				1.007
7	3	r	32	96.9	104.	125.5	-10.	97.	116.	-7.	112.	131.	-7.				1.007

v'	v"	J	E	N0	E0	D0	N1	E1	D1	N2	E2	D2	N3	E3	D3	Cov.
			(kV)	(1.)	(1.)	(1.5)	(1.)	(1.)	(1.5)	(1.)	(1.)	(1.5)	(1.)	(1.)	(1.5)	(0.002)
7	3	p	46	138.	141.5	163.5	-12.	145.	158.5	15.	161.	175.	17.	163.5	177.	17.	1.007
7	3	r	52	138.	122.5	145.	-14.	144.5	154.	17.	146.	157.	15.	147.	161.5	15.	1.007
9	4	r	65	138.	167.	173.5	9.	184.	97.5	106.	180.	95.	103.	188.5	102.	107.	1.007
9	4	p	59	138.	184.5	194.	8.	186.5	103.5	103.	191.	102.	109.	210.5	115.5	119.	1.007
7	3	p	46	96.9	141.5	163.5	-12.	149.5	167.	4.	145.5	162.5	5.				1.007
7	3	r	52	96.9	122.5	145.	-14.	143.5	161.	5.	131.	147.	4.				1.007
9	4	r	65	96.9	167.	173.5	9.	180.	124.5	73.	171.	121.	67.				1.007
9	4	p	59	96.9	184.5	194.	8.	192.5	133.5	78.	190.	132.	78.				1.007

v'	v"	J	E	N0	E0	D0	N1	E1	D1	N2	E2	D2	N3	E3	D3	Cov.
			(kV)	(1.)	(1.)	(1.5)	(1.)	(1.)	(1.5)	(1.)	(1.)	(1.5)	(1.)	(1.)	(1.5)	(0.01)
5	2	p	64	138.	58.	65.	0.	56.	53.	9.5	53.	50.	9.	57.	55.	9.	1.04
7	3	p	78	138.	142.	163.	-11.	138.	137.5	22.	138.	136.5	21.	144.	143.	23.	1.04
7	3	r	84	138.	123.5	140.5	-7.	120.	112.	20.	116.5	110.5	21.	123.5	118.	20.	1.04
9	4	r	92	138.	130.	135.	7.	124.	68.	68.	122.	60.	69.	139.	76.	77.	1.04
5	2	r	70	138.	55.	63.	0.	56.	52.5	10.	53.5	50.5	9.5	57.	54.	10.	1.04
9	4	p	86	138.	152.	155.	11.	156.	82.	90.	146.	76.	89.	164.	86.	96.	1.04
5	2	p	64	96.9	58.	65.	0.	57.	58.5	6.	56.	59.	3.				1.04
7	3	p	78	96.9	142.	163.	-11.	142.5	150.	7.	141.5	150.	7.				1.04
7	3	r	84	96.9	123.5	140.5	-7.	123.	125.	9.	122.	125.5	9.				1.04
9	4	r	92	96.9	130.	135.	7.	130.	90.	51.	130.	88.	54.				1.04
5	2	r	70	96.9	55.	63.	0.	57.	58.	3.	54.5	57.	3.				1.04
9	4	p	86	96.9	152.	155.	11.	154.	104.5	65.	153.	105.	63.				1.04
5	2	p	86	138.	46.	52.	0.	47.5	46.	6.	49.	50.	8.				1.04

9	4	p103	138.	130.	138.	0.	130.5	77.	66.	129.	76.	65.			1.04
5	2	p 86	96.9	46.	52.	0.	5.	48.5	1.5						1.04
9	4	p103	96.9	130.	138.	0.	130.	97.	45.5						1.04
7	3	p 93	138.	203.	230.	-8.	210.	188.	48.	210.	186.	51.			1.04
12	6	r 40	138.	34.	39.5	0.	37.	18.	23.	37.5	17.5	24.			1.04
10	5	r 29	138.	66.	72.	0.	70.	73.5	7.	70.	76.5	6.			1.04
10	5	p 23	138.	55.	59.	0.	55.	59.5	5.	57.5	63.	6.			1.04
7	3	p 93	96.9	203.	230.	-8.	212.	209.5	26.5	209.5	207.5	25.			1.04
12	6	r 40	96.9	34.	39.5	0.	32.	21.	15.	36.	23.5	17.			1.04
10	5	r 29	96.9	66.	72.	0.	70.5	77.5	3.	68.	75.	2.			1.04
10	5	p 23	96.9	55.	59.	0.	58.	63.	3.	56.5	61.5	3.			1.04
6	3	p 33	138.	108.5	120.5	0.	106.	54.	65.	103.	54.5	59.5			1.04
6	3	r 39	138.	126.5	141.5	0.	117.5	62.	69.5	113.5	59.	68.			1.04
9	4	p119	138.	41.	47.	0.	40.	25.	20.	38.5	25.	17.			1.04
6	3	p 33	96.9	154.5	169.	0.	128.	90.	53.	147.5	103.	60.5			1.04
6	3	r 39	96.9	169.5	187.	0.	149.	103.	64.	153.	107.	64.			1.04
9	4	p119	96.9	55.5	61.5	0.	49.	38.	16.5	55.	43.	18.			1.04

v′	v"	J	E (kV)	N0 (1.)	E0 (1.5)	D0 (2.5)	N1 (1.)	E1 (1.5)	D1 (2.5)	N2 (1.)	E2 (1.5)	D2 (2.5)	N3 (1.)	E3 (1.5)	D3 (2.5)	Cov. (0.01)
6	3	p 51	138.	128.	126.5	0.	125.5	64.	85.5	125.	65.	81.5				1.34
6	3	r 57	138.	138.	138.	0.	136.	70.	91.5	138.5	66.5	98.				1.34
8	4	r 72	138.	136.	142.	5.	131.	84.	63.5	134.5	86.	66.5				1.34
8	4	p 66	138.	149.5	157.5	5.	158.5	99.	82.	160.	102.5	82.				1.34
6	3	p 51	96.9	128.	126.5	0.	129.5	83.	62.5	116.5	75.	56.				1.34
6	3	r 57	96.9	138.	138.	0.	140.	90.	66.	127.	81.5	61.				1.34
8	4	r 72	96.9	136.	142.	5.	135.	107.5	36.5	122.	97.	34.				1.34
8	4	p 66	96.9	149.5	157.5	5.	167.	127.	54.	154.	116.	51.				1.34
6	3	p 87	138.	123.	121.5	0.	120.	59.	83.	119.	59.5	82.	127.5	66.	86.	1.34
4	2	p 72	138.	33.5	40.	0.	33.	19.5	20.	33.	16.	25.	33.5	18.5	22.	1.34
6	3	r 93	138.	101.	103.	0.	101.	50.5	68.	95.	50.	62.5	101.5	55.	64.	1.34
8	4	r102	138.	90.5	100.	-4.	89.	74.5	22.	87.	73.5	24.	95.	78.5	30.	1.34
8	4	p 96	138.	123.	131.	-5.	119.5	91.	39.	115.5	89.5	38.	125.5	98.5	38.	1.34
6	3	p 87	96.9	123.	121.5	0.	121.5	80.	58.	125.	77.	65.				1.34
4	2	p 72	96.9	33.5	40.	0.	33.	24.	13.	29.	21.	12.				1.34
6	3	r 93	96.9	101.	103.	0.	102.5	74.	42.	101.5	72.	43.				1.34
8	4	r102	96.9	90.5	100.	-4.	96.	86.	16.	93.	85.	17.				1.34
8	4	p 96	96.9	123.	131.	-5.	126.5	104.	31.	124.5	108.	25.				1.34

5	3	p	25	138.	130.5	133.	0.	126.	102.5	41.	124.	101.	38.	131.	100.	44.	1.34
5	3	r	31	138.	138.	146.	0.	140.	119.	41.	136.	115.5	39.	143.	119.	42.	1.34
8	4	r	126	138.	35.	35.	0.	34.	35.	6.	38.	29.5	5.	38.	33.	7.	1.34
5	3	p	24	138.	109.	120.	0.	110.5	91.	36.	109.	85.5	42.	116.	92.	40.	1.34
8	4	p	120	138.	51.5	53.5	0.	45.	47.	12.	45.	43.	6.	49.	45.	10.	1.34
5	3	p	25	96.9	130.5	133.	0.	126.5	116.	20.	124.	119.5	17.				1.34
5	3	r	31	96.9	138.	146.	0.	139.	130.	16.	135.	133.	19.				1.34
8	4	r	126	96.9	35.	35.	0.	34.5	35.	3.	30.5	35.	3.				1.34
5	3	p	24	96.9	109.	120.	0.	112.	99.	23.	114.5	102.5	24.				1.34
8	4	p	120	96.9	51.5	53.5	0.	49.5	52.5	5.	51.	49.	5.				1.34
5	3	p	50	138.	153.5	153.	0.	149.	126.	49.	150.	132.	45.	153.5	126.	47.	1.34
5	3	r	56	138.	154.5	163.	0.	154.5	133.	37.	150.5	135.	43.5	159.	138.	42.	1.34
7	4	p	68	138.	215.	224.	0.	205.	195.5	45.	212.	189.5	51.5	214.5	202.	46.	1.34
7	4	r	74	138.	199.	206.	0.	193.	172.	47.	192.5	178.	48.	197.5	179.	42.	1.34
5	3	p	50	96.9	153.5	153.	0.	154.5	136.5	34.	154.	142.5	30.				1.34
5	3	r	56	96.9	154.5	163.	0.	156.	143.	23.	157.	144.	32.				1.34
7	4	p	68	96.9	215.	224.	0.	215.	213.	19.	222.	212.5	20.				1.34
7	4	r	74	96.9	199.	206.	0.	194.	191.5	21.	196.5	193.	19.				1.34
5	3	p	93	138.	94.5	102.5	0.	93.5	93.	16.	95.	94.	18.	97.	97.5	15.	1.34
8	5	p	27	138.	133.	146.5	0.	131.5	74.5	81.	135.	76.	82.	133.5	83.5	80.	1.34
8	5	r	33	138.	160.	171.	0.	158.	92.5	95.	159.5	92.	98.	162.	92.5	102.5	1.34
5	3	r	99	138.	97.	98.5	0.	93.	92.5	20.	94.	98.	17.	98.	93.5	17.	1.34
8	5	p	26	138.	133.	131.	0.	128.5	71.5	80.	129.5	73.	83.	132.	75.5	81.5	1.34
8	5	r	32	138.	158.5	161.5	0.	153.	82.5	103.	151.	82.	111.5	159.5	91.	101.	1.34
5	3	p	93	96.9	94.5	102.5	0.	96.	97.	13.5	94.	102.	20.				1.34
8	5	p	27	96.9	133.	146.5	0.	136.	103.	57.5	138.5	102.	62.				1.34
8	5	r	33	96.9	160.	171.	0.	158.	116.5	65.	162.	121.	63.5				1.34
5	3	r	99	96.9	97.	98.5	0.	96.	98.	12.	92.	96.	13.				1.34
8	5	p	26	96.9	133.	131.	0.	130.	98.	52.	128.5	88.	59.5				1.34
8	5	r	32	96.9	158.5	161.5	0.	154.	112.	61.5	151.	111.	63.				1.34

v'	v"	J	E (kV)	N0 (2.)	E0 (3.)	D0 (4.)	N1 (2.)	E1 (3.)	D1 (4.)	N2 (2.)	E2 (3.)	D2 (4.)	N3 (2.)	E3 (3.)	D3 (4.)	Cov. (0.02)
4	4	r	34	138.	72.5	75.5	0.	70.5	44.	52.	74.5	41.	58.	73.	44.	47.	1.33
6	5	r	65	138.	132.	145.5	0.	126.	69.	87.	128.5	79.	77.	126.	70.	84.	1.33
4	4	p	27	138.	73.5	68.5	0.	75.5	43.	50.5	72.5	50.	50.	67.	36.	48.	1.33
4	4	r	33	138.	87.	83.	0.	92.5	50.	72.5	83.	51.	73.	82.	54.5	70.	1.33
4	4	p	26	138.	66.	68.	0.	62.5	35.5	53.	62.	38.	61.	62.5	40.	43.	1.33
4	4	r	34	96.9	72.5	75.5	0.	80.	51.	38.	77.	54.	41.				1.33

6	5	r	65	96.9	132.	145.5	0.	114.5	86.5	58.	130.5	82.	76.				1.33
4	4	p	27	96.9	73.5	68.5	0.	65.	55.	38.	73.5	47.	47.				1.33
4	4	r	33	96.9	87.	83.	0.	80.	58.	37.	82.	53.	59.				1.33
4	4	p	26	96.9	66.	68.	0.	65.	49.	35.	62.5	49.	31.5				1.33
4	4	r	52	138.	87.5	97.	0.	87.	44.	71.	82.	48.	60.	94.5	42.	75.	1.33
6	5	p	69	138.	128.	129.	0.	140.	77.	94.	133.	79.	83.	136.5	71.	97.	1.33
4	4	p	45	138.	109.5	114.	0.	109.5	59.	92.	104.5	58.	86.	112.	62.	81.	1.33
6	5	r	75	138.	132.	127.	0.	121.	65.	86.	122.	59.	94.	123.	73.	80.	1.33
4	4	r	51	138.	113.	101.	0.	103.	56.	81.	100.	50.	84.	106.5	57.	77.	1.33
4	4	r	52	96.9	87.5	97.	0.	88.	62.	53.	87.	57.	50.				1.33
6	5	p	69	96.9	128.	129.	0.	141.5	97.	70.	132.	94.	66.				1.33
4	4	p	45	96.9	109.5	114.	0.	106.	76.	54.	102.	74.	63.				1.33
6	5	r	75	96.9	132.	127.	0.	128.	81.	72.	124.5	77.	76.				1.33
4	4	r	51	96.9	113.	101.	0.	107.	67.	62.	106.	67.	63.				1.33

v'	v"	J	E (kV)	N0 (3.)	E0 (4.)	D0 (6.)	N1 (3.)	E1 (4.)	D1 (6.)	N2 (3.)	E2 (4.)	D2 (6.)	N3 (3.)	E3 (4.)	D3 (6.)	Cov. (0.02)
7	6	p	26	138.	108.	87.	30.	107.	79.	65.	101.	83.	70.	88.	82.	66.	1.28
6	5	p	103	138.	167.5	146.	73.	155.5	97.	120.	163.	88.	120.	165.5	85.	130.	1.28
7	6	p	25	138.	122.	107.	55.	135.	102.	72.	110.5	97.	72.	121.	105.	56.	1.28
4	4	p	89	138.	154.5	127.	58.	150.	66.	131.	153.	70.	148.	170.	83.5	157.	1.28
7	6	r	31	138.	135.5	111.	68.	129.	104.	75.	147.5	90.	101.	132.	115.	62.	1.28
7	6	p	26	96.9	108.	87.	30.	97.	92.	38.	91.5	83.	42.				1.28
6	5	p	103	96.9	167.5	146.	73.	151.	109.	80.	171.	103.	115.				1.28
7	6	p	25	96.9	122.	107.	55.	137.5	104.	74.	138.5	104.	77.				1.28
4	4	p	89	96.9	154.5	127.	58.	158.5	79.	144.	155.	82.	126.				1.28
7	6	r	31	96.9	135.5	111.	68.	133.	112.	62.	142.	121.	76.				1,28

Appendix B

Calculated predissociation rate from experiment data

The electric field induced predissociation rate constants calculated from the data in appendix A are listed here. In the column Gamma are calculated total decay rate Γ_T in the unit of $\frac{1}{s}$. The unit of electric field strength is kV/cm. The unit of β_1, β_2 and β_3 are $cm^2kV^{-2}s^{-1}$. For each given transition, the first two lines of data give those βs calculated by RATIO method; the last two lines of data are those calculated by DIFFERENCE method and are not used in analysis of data.

v' v" J	Gamma (1/s)	E (kV/cm)	beta1	beta2	beta3	ave. err.
4-4 p 26	2.71e+06	138.	115	96	86	99 +- 16
from RATIO method		96.9	106	91		98 +- 8
		138.	197	212	142	184 +- 42
from DIFFERENCE method		96.9	192	173		182 +- 10
4-4 p 27	3.33e+06	138.	111	61	128	100 +- 39
		96.9	36	162		99 +- 63
		138.	191	162	217	190 +- 27
		96.9	229	331		280 +- 51
4-4 r 33	3.44e+06	138.	138	99	78	105 +- 32
		96.9	116	174		145 +- 29
		138.	243	240	215	233 +- 17

		96.9	218	380		299 +- 81
4-4 r 34	2.85e+06	138.	100	133	108	114 +- 19
		96.9	192	147		170 +- 23
		138.	164	196	148	170 +- 27
		96.9	211	215		213 +- 2
4-4 p 45	3.72e+06	138.	181	170	171	174 +- 7
		96.9	179	172		176 +- 3
		138.	283	269	237	263 +- 26
		96.9	262	314		288 +- 26
4-4 r 51	3.89e+06	138.	131	160	136	142 +- 18
		96.9	177	171		174 +- 3
		138.	274	318	256	283 +- 36
		96.9	357	363		360 +- 3
4-4 r 52	3.31e+06	138.	206	155	258	206 +- 52
		96.9	202	244		223 +- 21
		138.	260	201	288	250 +- 48
		96.9	281	288		284 +- 4
4-2 p 72	4.04e+06	138.	215	309	245	256 +- 52
		96.9	276	279		278 +- 2
		138.	201	306	233	246 +- 59
		96.9	216	228		222 +- 6
4-4 p 89	5.45e+06	138.	247	227	192	222 +- 30
		96.9	377	322		349 +- 28
		138.	305	355	327	329 +- 26
		96.9	612	467		540 +- 73
5-3 p 24	2.79e+06	138.	49	59	57	55 +- 6

		96.9	73	68		71 +- 2
		138.	54	66	59	60 +- 7
		96.9	64	65		64 +- 0
5-3 p 25	3.46e+06	138.	46	45	61	51 +- 10
		96.9	41	21		31 +- 10
		138.	67	63	74	68 +- 6
		96.9	59	49		54 +- 5
5-3 r 31	3.57e+06	138.	46	46	51	47 +- 3
		96.9	50	28		39 +- 11
		138.	60	58	61	60 +- 1
		96.9	43	50		47 +- 3
5-3 p 50	3.40e+06	138.	32	24	38	31 +- 8
		96.9	46	28		37 +- 9
		138.	64	56	62	61 +- 4
		96.9	84	71		77 +- 6
5-3 r 56	3.61e+06	138.	43	33	41	39 +- 6
		96.9	58	58		58 +- 0
		138.	49	56	53	53 +- 4
		96.9	57	79		68 +- 11
5-2 p 64	3.91e+06	138.	38	38	33	36 +- 3
		96.9	38	27		32 +- 6
		138.	44	44	40	42 +- 3
		96.9	51	25		38 +- 13
5-2 r 70	4.16e+06	138.	48	46	46	47 +- 2
		96.9	56	42		49 +- 7
		138.	49	49	48	49 +- 1

		96.9	27	28		28 +- 0
5-2 p 86	4.95e+06	138.	43	28		36 +- 8
		96.9	26			26 +- 0
		138.	40	49		45 +- 5
		96.9	19			19 +- 0
5-3 p 93	6.00e+06	138.	28	30	25	28 +- 3
		96.9	47	-0		23 +- 24
		138.	50	56	45	50 +- 6
		96.9	82	116		99 +- 17
5-3 r 99	6.37e+06	138.	7	-9	21	7 +- 15
		96.9	-4	-18		-11 +- 7
		138.	67	54	56	59 +- 8
		96.9	77	85		81 +- 4
6-3 p 33	3.50e+06	138.	216	201		209 +- 7
		96.9	207	211		209 +- 2
		138.	262	238		250 +- 12
		96.9	261	260		261 +- 0
6-3 r 39	3.63e+06	138.	213	219		216 +- 3
		96.9	231	223		227 +- 4
		138.	253	260		257 +- 4
		96.9	286	275		281 +- 5
6-3 p 51	3.96e+06	138.	194	187		190 +- 4
		96.9	229	226		227 +- 1
		138.	257	241		249 +- 8
		96.9	295	292		293 +- 1
6-3 r 57	4.16e+06	138.	205	236		220 +- 15

		96.9	246	248		247 +- 1
		138.	264	297		280 +- 17
		96.9	301	308		304 +- 3
6-5 r 65	4.46e+06	138.	236	185	229	217 +- 32
		96.9	218	358		288 +- 70
		138.	274	212	261	249 +- 37
		96.9	297	411		354 +- 57
6-5 p 69	4.62e+06	138.	201	168	227	199 +- 30
		96.9	232	205		218 +- 14
		138.	275	237	308	273 +- 36
		96.9	331	322		327 +- 4
6-5 r 75	4.89e+06	138.	202	253	159	205 +- 48
		96.9	271	289		280 +- 9
		138.	315	380	261	319 +- 61
		96.9	431	479		455 +- 24
6-2 p 84	4.69e+06	138.	280	278	280	279 +- 2
		96.9	326	318		322 +- 4
		138.	206	205	198	203 +- 5
		96.9	234	219		226 +- 8
6-3 p 87	5.48e+06	138.	289	280	260	276 +- 16
		96.9	292	352		322 +- 30
		138.	374	366	346	362 +- 16
		96.9	392	457		424 +- 32
6-3 r 93	5.81e+06	138.	316	285	268	289 +- 26
		96.9	255	271		263 +- 8
		138.	379	352	328	353 +- 26

		96.9	326	343		334 +- 9
6-5 p103	6.40e+06	138.	133	206	234	191 +- 58
		96.9	142	305		223 +- 82
		138.	157	173	218	183 +- 35
		96.9	42	270		156 +-114
7-6 p 25	3.16e+06	138.	27	-0	2	9 +- 17
		96.9	54	57		55 +- 1
		138.	27	28	2	19 +- 17
		96.9	60	69		64 +- 5
7-6 p 26	2.60e+06	138.	12	-3	-18	-3 +- 15
		96.9	-42	-31		-36 +- 5
		138.	58	63	58	60 +- 4
		96.9	23	39		31 +- 8
7-3 p 28	2.63e+06	138.	10	11	10	10 +- 0
		96.9	9	13		11 +- 2
		138.	33	33	-3	21 +- 24
		96.9	-2	-4		-3 +- 1
7-3 p 29	3.23e+06	138.	7	6	4	6 +- 2
		96.9	-0	3		1 +- 1
		138.	37	41	-4	25 +- 29
		96.9	-4	-8		-6 +- 2
7-6 r 31	3.26e+06	138.	3	58	-10	17 +- 41
		96.9	-9	-13		-11 +- 2
		138.	11	61	-9	21 +- 40
		96.9	-18	22		2 +- 20
7-3 r 32	2.70e+06	138.	4	7	5	5 +- 2

		96.9	3	9		6 +- 3
		138.	23	23	6	17 +- 11
		96.9	9	8		9 +- 1
7-3 r 33	3.30e+06	138.	13	10	8	10 +- 3
		96.9	5	9		7 +- 2
		138.	37	38	0	25 +- 25
		96.9	3	-3		0 +- 3
7-3 p 46	3.02e+06	138.	9	10	11	10 +- 1
		96.9	11	11		11 +- 0
		138.	33	32	32	32 +- 1
		96.9	38	41		40 +- 2
7-3 r 52	3.19e+06	138.	18	17	13	16 +- 3
		96.9	19	19		19 +- 0
		138.	41	38	37	39 +- 3
		96.9	49	51		50 +- 1
7-4 p 68	3.74e+06	138.	18	32	21	24 +- 9
		96.9	21	35		28 +- 7
		138.	42	49	41	44 +- 5
		96.9	33	35		34 +- 1
7-4 r 74	3.99e+06	138.	34	25	30	29 +- 4
		96.9	21	23		22 +- 1
		138.	53	52	45	50 +- 5
		96.9	43	39		41 +- 2
7-3 p 78	4.16e+06	138.	33	35	34	34 +- 1
		96.9	40	37		38 +- 2
		138.	61	60	61	61 +- 1

		96.9	62	62		62 +- -0
7-3 r 84	4.44e+06	138.	51	46	44	47 +- 4
		96.9	57	50		53 +- 3
		138.	67	70	63	67 +- 3
		96.9	72	72		72 +- 0
7-3 p 93	5.49e+06	138.	76	80		78 +- 2
		96.9	86	84		85 +- 1
		138.	102	108		105 +- 3
		96.9	114	111		113 +- 2
8-5 p 26	2.08e+06	138.	84	81	79	81 +- 3
		96.9	68	97		83 +- 15
		138.	113	115	109	112 +- 3
		96.9	109	139		124 +- 15
8-5 p 27	2.51e+06	138.	124	126	100	116 +- 17
		96.9	122	133		127 +- 6
		138.	132	131	117	127 +- 10
		96.9	138	151		144 +- 6
8-3 p 31	2.55e+06	138.	110	112	111	111 +- 1
		96.9	125	109		117 +- 8
		138.	77	79	76	77 +- 2
		96.9	51	41		46 +- 5
8-5 r 32	2.15e+06	138.	100	98	88	96 +- 7
		96.9	92	88		90 +- 2
		138.	130	142	116	129 +- 13
		96.9	116	120		118 +- 2
8-5 r 33	2.58e+06	138.	111	115	118	115 +- 3

		96.9	123	118		121 +- 3
		138.	128	133	138	133 +- 5
		96.9	142	134		138 +- 4
8-3 r 37	2.63e+06	138.	109	105	103	106 +- 3
		96.9	118	118		118 +- 0
		138.	81	76	74	77 +- 4
		96.9	52	48		50 +- 2
8-4 p 66	2.78e+06	138.	100	94		97 +- 3
		96.9	114	118		116 +- 2
		138.	105	101		103 +- 2
		96.9	106	109		107 +- 1
8-4 r 72	2.93e+06	138.	96	97		97 +- 0
		96.9	97	98		98 +- 0
		138.	99	102		100 +- 1
		96.9	85	87		86 +- 1
8-3 p 93	4.00e+06	138.	77	76	79	77 +- 2
		96.9	71	74		73 +- 1
		138.	62	61	64	62 +- 2
		96.9	62	60		61 +- 1
8-4 p 96	3.69e+06	138.	77	72	69	73 +- 4
		96.9	116	90		103 +- 13
		138.	87	86	78	84 +- 5
		96.9	126	101		114 +- 12
8-3 r 99	4.22e+06	138.	63	62	71	66 +- 6
		96.9	77	70		74 +- 3
		138.	52	52	59	54 +- 5

		96.9	68	57		63 +- 5
8-4 r102	3.92e+06	138.	66	63	69	66 +- 3
		96.9	97	87		92 +- 5
		138.	66	72	82	74 +- 9
		96.9	90	96		93 +- 3
8-3 p103	4.37e+06	138.	64	63	58	62 +- 3
		96.9	65	65		65 +- 0
		138.	83	86	78	82 +- 4
		96.9	85	80		82 +- 2
8-4 p120	4.67e+06	138.	-1	21	32	17 +- 19
		96.9	-10	40		15 +- 25
		138.	58	32	50	47 +- 15
		96.9	44	47		45 +- 2
8-4 r126	4.94e+06	138.	-7	74	39	35 +- 43
		96.9	-8	-68		-38 +- 30
		138.	41	41	51	44 +- 7
		96.9	42	42		42 +- -0
9-4 p 25	1.89e+06	138.	85	84	84	84 +- 1
		96.9	90	94		92 +- 2
		138.	109	102	107	106 +- 4
		96.9	115	116		116 +- 1
9-4 r 30	1.66e+06	138.	80	80	78	79 +- 1
		96.9	85	84		84 +- 0
		138.	100	97	99	99 +- 2
		96.9	108	104		106 +- 2
9-4 r 31	1.94e+06	138.	92	93	91	92 +- 1

		96.9	99	97		98 +- 1
		138.	114	114	115	114 +- 1
		96.9	126	123		125 +- 1
9-4 p 46	1.84e+06	138.	101	98	96	98 +- 3
		96.9	104	109		107 +- 3
		138.	123	123	123	123 +- 0
		96.9	134	139		137 +- 3
9-4 r 52	1.92e+06	138.	10	105	96	100 +- 4
		96.9	111	113		112 +- 1
		138.	123	122	122	122 +- 1
		96.9	143	140		142 +- 2
9-4 p 59	2.30e+06	138.	107	116	110	111 +- 5
		96.9	126	126		126 +- 0
		138.	136	146	142	141 +- 6
		96.9	158	160		159 +- 1
9-4 r 65	2.40e+06	138.	121	122	116	119 +- 4
		96.9	128	120		124 +- 4
		138.	154	153	149	152 +- 3
		96.9	162	151		156 +- 5
9-4 p 86	2.59e+06	138.	127	130	128	128 +- 2
		96.9	139	134		136 +- 2
		138.	155	165	159	160 +- 5
		96.9	169	162		166 +- 4
9-4 r 92	2.74e+06	138.	128	159	129	139 +- 21
		96.9	146	156		151 +- 5
		138.	153	176	157	162 +- 14

		96.9	170	185		178 +- 8
9-4 p103	3.31e+06	138.	138	139		138 +- 0
		96.9	149			149 +- 0
		138.	176	176		176 +- 0
		96.9	196			196 +- 0
9-3 p110	3.25e+06	138.	143	166	144	151 +- 15
		96.9	142	174		158 +- 16
		138.	175	209	182	188 +- 20
		96.9	163	193		178 +- 15
9-4 p119	3.81e+06	138.	166	152		159 +- 7
		96.9	174	169		172 +- 2
		138.	189	161		175 +- 14
		96.9	210	202		206 +- 4
10-5 p 23	1.60e+06	138.	-1	-2		-1 +- 1
		96.9	-2	-2		-2 +- 0
		138.	8	9		9 +- 1
		96.9	1	1		1 +- 0
10-5 r 29	1.63e+06	138.	3	-0		2 +- 2
		96.9	-1	-2		-2 +- 0
		138.	1	8		9 +- 1
		96.9	8	6		7 +- 1
10-4 p 45	1.74e+06	138.	5	4	5	5 +- 0
		96.9	11	1		10 +- 1
		138.	10	1	14	11 +- 2
		96.9	11	11		11 +- 0
10-4 r 51	1.80e+06	138.	3	5	6	5 +- 2

		96.9	10	8		9 +- 1
		138.	11	12	14	12 +- 2
		96.9	13	11		12 +- 1
10-4 p 98	2.27e+06	138.	30	31	25	28 +- 4
		96.9	24	38		31 +- 7
		138.	24	25	17	22 +- 5
		96.9	18	27		23 +- 4
10-4 p107	2.65e+06	138.	66	64	59	63 +- 4
		96.9	76	74		75 +- 1
		138.	82	77	79	79 +- 3
		96.9	95	87		91 +- 4
12-6 r 40	9.16e+05	138.	66	71		69 +- 2
		96.9	75	76		76 +- 0
		138.	73	78		75 +- 3
		96.9	83	84		83 +- 1

Appendix C

The wave function solution of a straight line potential

Assume C potential curve is a straight line and pass the two points:

$$\mathrm{x = b} \quad \mathrm{U} = \epsilon$$

$$\mathrm{x = R} \quad \mathrm{U} = 0$$

Then the line equation is:

$$U = -Fx + B \tag{C.82}$$

where $F = \frac{\epsilon}{R-b}$ and $B = FR$. The schrödinger equation is:

$$\frac{\hbar^2}{2\mu}\frac{d^2\Psi}{dx^2} + [E - U]\Psi = 0 \tag{C.83}$$

where μ is reduced mass, E is the total energy, U is the potential energy. Substitute into the Eq. C.82 we get:

$$\frac{d^2\Psi}{dx^2} = -\left[x + \frac{E-B}{F}\right]\left(\frac{2\mu F}{\hbar^2}\right)\Psi = 0 \tag{C.84}$$

The solution for Eq: C.84 is[3]:

$$\Psi(y) = A\Upsilon(-y) \tag{C.85}$$

where

$$y = -\left[x + \frac{E-B}{F}\right]\left(\frac{2\mu F}{\hbar^2}\right)^{\frac{1}{3}} \tag{C.86}$$

$$\Upsilon(-y) = Airy(-y) \tag{C.87}$$

The above equations should be equivalent to semiclassical theory when y is large.

Bibliography

[1] J. C. Lehmann, *Iodine, a test molecule in modern spectroscopy, Contemp. Phys.* **19**, No. 5, 449-468, (1978)

[2] G. Herzberg, *Molecular spectra and molecular structure*, second edition, (1950)

[3] L. D. Landau and E. M. Lifshitz *Quantum mechanics*, third edition, (Pergamon press, Oxford, 1977)

[4] M. S. Child, *Semi-classical analysis of weakly inelastic molecular collisiona, Mol. Phys.* **8**, 517-531, (1964)

[5] M. S. Child, *Repulsive potential curves from predisociation data, J. Mol. Phys.* **33**, 487-493, (1970)

[6] D. S. Ramsay and M. S. Child, *Analytical theory of fluctuations in the predissociation linewidth, Mol. Phys.* **22**, 263-271, (1971)

[7] M. S. Child, *Direct inversion of magnetic flourescence quenching data for the* $B^3\Pi_{0_u^+}$ *state of iodine, J. Mol. Spectrosc.* **45**, 293-297, (1973)

[8] M. S. Child, *Predissociation and photodissociation of IBr: A case of intermediate coupling strength, Mol. Phys.* **32**, No. 6, 1495-1510, (1976)

[9] M. S. Child, *Analytical interpretation of predisociation rates: the* $B\,^3\Pi_{0_u^+}$ *state of* Br_2, *J. Phys. B: Atom. Molec. Phys.*, **13**, 2557-2563, (1980)

[10] F. W. Dalby, C. D. P. Levy and J. Vanderlinde, *Vibrational and rotational dependence of electric field induced predissociation of* I_2 , *Chem. Phys* **85**, No. 1, (1984)

[11] I. S. Gradshteyn and I. M. Ryzhik, *Table of integrals, series, and products*, corrected and enlarged edition, P399.

[12] R. F. Barrow and K. K. Yee, $B\,^3\Pi_{0_u^+}$ - $X\,^1\Sigma_g^+$ *system of* $^{127}I_2$*: rotational analysis and long range potential in the* $B\,^3\Pi_{0_u^+}$ *state, J. Chem. Soc. Faraday Trans. II* **69**, p684, (1973)

[13] C. D. Hodgman *et al. Handbook of chemistry and physics*, 39th edition, (Chemical Rubber Publishing Co., Ohio 1957-1958)

[14] J. L. Booth, F. W. Dalby, S. Parmar and J. Vanderlinde, *Ortho-para iodine separation revisited, Chem. Phys.* **132**, P209-217, (1989)

[15] S. Gerstenkorn and P. Luc, *Atlas du spectre d'Absorption de la molecule d'iode* (C. N. R. S., Paris,1977)

[16] J. Vigué, M. Broyer and J. C. Lehmann, *Natural haperfine and magnetic predissociation of the* I_2 *B state, I., J. Physique* **42**, P937-947, (1981)

[17] J. Vigué, M. Broyer and J. C. Lehmann, *Natural haperfine and magnetic predissociation of the* I_2 *B state, II., J. Physique* **42**, P949-959, (1981)

[18] J. Vigué, M. Broyer and J. C. Lehmann, *Natural haperfine and magnetic predissociation of the* I_2 *B state, III., J. Physique* **42**, P960-978, (1981)

[19] B. J. Sullivan and D. A. Dows, *Electric field-induced predissociation of* I_2 *(*$B\,^3\Pi_{0_u^+}$ *) Chem. Phys.* **46**, P231-236, (1980)

[20] C. Zener, *Proc. Roy. Soc.* **A140**, 660, (1933)

[21] R. S. Mulliken, *Iodine Revisitd, J. Chem. Phys.* **55**, P289, (1971)

[22] J. Vigué, THESIS DE DOCTORAT D'ETAT, UNIVERSITÉ DE PARIS. P222. (1978)

[23] S. Gerstenkorn and P. Luc, *Discription of the absorption spectrum of iodine recorded by means of Fourier Transform Spectroscopy: the (B-X) system J. Physique* **46**, P867-881, (1985)